Serotonergic signaling controls input-specific synaptic plasticity at striatal circuits

Marta Gritti[1], Andrea Giorgi[2,4], Anna Cavaccini[1], Massimo Trusel[1], Sara Migliarini[2], Tiziano Catelani[3], Roberto Marotta[3], Alessandro Gozzi[4], Massimo Pasqualetti[2,4,5] & Raffaella Tonini[1*]

[1]*Neuroscience and Brain Technologies Department, Istituto Italiano di Tecnologia, Genova, Italy*

[2] *Department of Biology, Unit of Cell and Developmental Biology, University of Pisa, Pisa, Italy*

[3]*Nanochemistry Department, Istituto Italiano di Tecnologia, Genova, Italy*

[4]*Center for Neuroscience and Cognitive systems, Istituto Italiano di Tecnologia, Rovereto, Italy*

[5]*Neuroscience Institute, National Research Council (CNR), Pisa, Italy*

***Corresponding author**

Raffaella Tonini (raffaella.tonini@iit.it)

Running title

Serotonin controls plasticity at thalamostriatal inputs

Abstract

Monoaminergic modulation of cortical and thalamic inputs to the dorsal striatum (DS) is crucial for reward-based learning and action control. While dopamine in this context has been extensively investigated, the synaptic effects of serotonin (5-HT) are largely unexplored. In this study, we investigated how serotonergic signaling affects associative plasticity at glutamatergic synapses on the striatal projection neurons of the direct pathway (dSPNs). Combining chemogenetic and optogenetic approaches reveals that impeding serotonergic signaling gates spike-timing-dependent long-term depression (t-LTD) preferentially at thalamostriatal synapses. This form of t-LTD requires dampened activity of the 5-HT4-receptor subtype, which we demonstrate controls dendritic Ca^{2+} signals through the regulation of BK channel activity. This represents a novel synaptic mechanism underpinning the 5-HT modulation of dSPNs. The synaptic effects of decreased 5-HT signaling at thalamostriatal inputs provides new mechanistic insights into how changes in serotonergic levels associated with behavioral states or pathology may affect striatal-dependent processes.

Introduction

The dorsal striatum (DS) of the basal ganglia (BG) plays a critical role in voluntary movement, learning and motivation. It also represents the primary site of dysfunction in psychomotor diseases such as Parkinson's disease (PD), drug addiction and obsessive-compulsive disorders (OCD). The DS receives glutamatergic excitatory inputs from the cortex and the thalamus. These inputs converge on striatal projection neurons (SPNs) of the direct (dSPN) and indirect (iSPN) pathways, which exert opposing control over motor output and hedonic states. While dSPNs stimulate movement, reinforcement and reward, iSPNs inhibit movement and mediate punishment and aversion (Bateup et al., 2010; Kravitz et al., 2010; Kravitz et al., 2012; Tecuapetla et al., 2016; Vicente et al., 2016)

It is increasingly clear that encoding of action selection at striatal circuits requires regulation of SPN activity and plasticity (Kravitz et al., 2012; Nazzaro et al., 2012; O'Hare et al., 2016; Sippy et al., 2015). One of the most important neuromodulatory inputs to the striatum is dense dopaminergic innervation from the substantia nigra (Tritsch et al., 2012). In particular, dSPNs expressing the Gs-coupled D1 dopamine (DA) receptors are stimulated by dopaminergic signaling. In the presence of behaviorally relevant stimuli, DA is assumed to reinforce motor actions that result in reward outcomes through the potentiation of corticostriatal synapses formed on dSPNs (Gerfen and Surmeier, 2011). Recent evidence indicates that DA depletion specifically weakens thalamic connections to dSPNs but not cortical afferents to these neurons (Parker et al., 2016). This weakening, which does not occur in iSPNs, is directly associated with motor abnormalities.

In addition to the dopaminergic afferents, serotonergic inputs from the medial and dorsal raphe nucleus (DRN) modulate the activity of SPNs, affecting striatal function and consequently behaviors, including motor and motivational goal-directed behavior (Mathur and Lovinger, 2012). Serotonergic neurons of the DRN fire coincidently with the initiation and termination of selected voluntary movements, whereas reduction in DRN activity to levels at or below baseline is associated with pauses in motor sequences (Fornal et al., 1996; Jacobs and Fornal, 1999). The

evidence of striatal serotonin (5-HT) influencing action control is consistent with dysfunction of the 5-HT system described in OCD, and with the use of Selective Serotonin Reuptake Inhibitors (SSRI) for the treatment of this disorder (Goddard et al., 2008).

In the DS, 5-HT acts on diverse receptors that are expressed on both presynaptic and postsynaptic circuit elements (Mathur and Lovinger, 2012). Depending on their localization, striatal 5-HT receptors initiate transduction through several Gi/o-, Gq/11- and Gs protein-dependent- and independent pathways (Hannon and Hoyer, 2008). The specific responses to 5-HT may be also contingent upon cross-talk with other receptor types. In dSPNs, the temporal, combinational logic of serotonergic and D1R-mediated signaling may shape the net synaptic output depending on the relative balance of these two neuromodulators. It has been reported that increased concentrations of 5-HT in the striatum reduce glutamate release at corticostriatal afferents by activating the presynaptic Gi-coupled 5-HT1b receptors (Mathur et al., 2011). 5-HT can also facilitate the release of DA from dopaminergic projections (Navailles and De Deurwaerdere, 2011). In contrast, despite their potential implications for BG function and pathological conditions characterized by hypo serotonergic states, the synaptic effects of reduced striatal 5-HT signaling remain unexplored. Neither it is known whether there is any input specificity of 5-HT modulation at corticostriatal and thalamostriatal synapses.

In this study, we investigated the effect of impeding 5-HT release, thereby serotonergic signaling, on timing-dependent synaptic plasticity in dSPNs, and describe a novel cellular mechanism that underlies the input-specific impact of 5-HT at thalamostriatal synapses.

Results

Chemogenetic inhibition of 5-HT release gates t-LTD at glutamatergic afferents to dSPNs

To test how plasticity is modulated at glutamatergic inputs on dSPNs of the dorsolateral striatum (DLS), we recorded excitatory postsynaptic potentials (EPSPs) following intrastriatal stimulation. Intrastriatal stimulation is likely activating cortical and thalamic afferents as well as dopaminergic and serotonergic fibers (**Figure 1**)(Shen et al., 2015; Threlfell et al., 2012; Wu et al., 2015). dSPNs were selected through their negative resting membrane potential and firing properties (Kreitzer and Malenka, 2007; Nazzaro et al., 2012). After recording, dSPN cell identity was confirmed by immunostaining for the specific marker substance P, and the lack of immunoreactivity for the iSPN marker A2A (**Figure 1A**) (Nazzaro et al., 2012; Trusel et al., 2015). We investigated long-lasting changes in EPSPs induced upon a spike-timing-dependent plasticity paradigm (STDP) (Nazzaro et al., 2012; Shen et al., 2008). As previously shown (Shen et al., 2008; Shen et al., 2015), a post-pre STDP protocol (**Figure 1B**), in which the postsynaptic spike precedes the presynaptic stimulation, did not induce plasticity in this SPN subpopulation (96 ± 4 % of baseline, $n = 8$, $p > 0.05$; **Figure 1B**). Previous studies show that this STDP protocol leads to long-term synaptic depression (t-LTD) in dSPNs when either dopamine D1 receptors (D1R) are inhibited or striatal DA is depleted (Shen et al., 2008; Shen et al., 2015). The effects of decreased 5-HT signaling at glutamatergic dSPN synapses during STDP, however, remains to be determined. To address this question, we manipulated 5-HT release chemogenetically. We used a newly generated transgenic DREADD (Designer Receptors Exclusively Activated by Designer Drugs) mouse line ($hM4Di^{+/-}$/$Pet1_{210}$-Cre) obtained by crossing the $Pet1_{210}$-Cre transgenic mouse line (Pelosi et al., 2014) with the hM4Di knock-in mice expressing the DREADD receptor hM4Di fused in frame with the mCherry reporter and flanked by two sets of Lox sites (i.e. LoxP/Lox2722) (**Figure S1A**). Upon Cre-mediated somatic recombination, the double floxed DREADD sequence is effectively inverted, leading to transcription of the inhibitory DREADD receptor hM4Di in $Pet1_{210}$-expressing 5-HT neurons; in brain slices from $hM4Di^{+/-}$/$Pet1_{210}$-Cre mice, these neurons can be identified by the

expression of the mCherry reporter (**Figure S1B** and **Figure S2A-I**). We first confirmed that the hM4Di receptor silenced serotonergic neurons of the dorsal raphe nucleus (DRN) when activated by its cognate ligand clozapine-N-oxide (CNO; **Figure S1C-F**). Bath application of CNO (5 μM) significantly decreased the firing discharge of $mCherry^{positive}$ but not $mCherry^{negative}$ neurons (**Figure S1D-E**). CNO did not affect the firing rate of DRN 5-HT neurons from $hM4Di^{+/-}$ littermates negative for $Pet1_{210}$-Cre (**Figure S1F**). mCherry- and 5-HT co-immunoreactivity was verified in the DLS of $hM4Di^{+/-}$/$Pet1_{210}$-Cre mice by immunoelectron microscopy (**Figure S2J-L**). We then assessed whether CNO application in the DLS of $hM4Di^{+/-}$/$Pet1_{210}$-Cre mice affected plasticity outcomes (**Figure 1**). In dSPNs from these mice, t-LTD was observed following the STDP protocol in the presence of CNO but not in the control (5 μM; 74 ± 4% of baseline, $n = 8$, $p < 0.05$ versus 95 ± 5% of baseline, $n = 5$, $p > 0.05$; **Figure 1C**). No changes in synaptic responses were observed when CNO was applied during STDP in naïve mice (92 ± 6% of baseline, $n = 7$, $p > 0.05$, **Figure S3A**).

Together, these results indicate that the chemogenetic inhibition of 5-HT release in the DLS gates t-LTD at glutamatergic afferents to dSPNs.

Antagonism of 5-HT4R signaling enables t-LTD in dSPNs

Our findings indicate that 5-HT, similar to DA through the Gs-coupled D1R (Shen et al., 2008), disrupts the induction of t-LTD in dSPNs. To elucidate the molecular mechanism underlying this role, we tested whether inhibiting 5-HT Gs-mediated signaling allows t-LTD to occur. The striatum contains a high density of the 5-HT6R and 5-HT4R subtypes, which, like D1R, are coupled to Gs, and are expressed in SPNs (Di Matteo et al., 2008; Eskenazi et al., 2015; Vilaro et al., 1996). Bath perfusion of the 5-HT6R antagonist SB271046 (5 μM) during the post-pre protocol did not promote plasticity in dSPNs (SB271046, 99 ± 8% of baseline, $n = 6$, $p > 0.05$, **Figure S3B**). In contrast, delivering the post-pre STDP paradigm in the presence of the 5-HT4R antagonists

GR113808 (5 μM) or RS39604 (5 μM) revealed t-LTD in the same neuronal subpopulation (GR113808, 79 ± 5% of baseline, n = 8, $p < 0.05$; RS39604, 68 ± 4% of baseline, n = 10, $p < 0.05$; **Figure 2A**). Thus, 5-HT4R inhibition recapitulated the synaptic effects of chemogenetic inhibition of 5-HT release. Application of either antagonist in the absence of the pairing protocol did not affect glutamatergic synaptic transmission, confirming that coordinated postsynaptic and presynaptic activity is necessary for the induction of t-LTD (GR113808, 94 ± 5% of baseline, n = 5, $p > 0.05$; RS39604, 96 ± 4% of baseline, n = 6, $p > 0.05$; **Figure S3C**).

Previous studies demonstrated that in dSPNs, antagonism of the Gs-coupled D1R signaling allows endocannabinoid (eCB) biosynthesis, ultimately leading to LTD that is mediated by the activation of the presynaptic cannabinoid receptor CB1 (Shen et al., 2008; Shen et al., 2015). This was not the case for antagonism of 5-HT4R signaling, as the co-application of RS39604 with the CB1R antagonist AM251 (4 μM) did not prevent t-LTD induction (RS39604 + AM251, 62 ± 7 % of baseline, n = 5, $p < 0.05$; **Figure 2B**). We then investigated the locus of plasticity expression by recording synaptic responses generated by twin stimuli, before and after the STDP protocol. In this set of experiments, we found that t-LTD was enabled by antagonism of 5-HT4R (RS39604, 77 ± 5% of baseline, n = 6, $p < 0.05$; **Figure 2C**) but was not accompanied by a change in paired-pulse-ratio (PPR), a hallmark of presynaptic plasticity (PPR: $before_{STDP}$, 1.33 ± 0.09; $after_{STDP}$, 1.35 ± 0.11, $p > 0.05$; **Figure 2C**). This raises the possibility that this form of LTD is expressed post-synaptically. Consistent with this, the intracellular dialysis of the peptide D15 (1.5 mM), which prevents postsynaptic AMPAR endocytosis (Carroll et al., 1999a; Carroll et al., 1999b; Morishita et al., 2005), blocked t-LTD expression (RS39604/D15, 91 ± 5% of baseline, n = 8, $p > 0.05$; **Figure 2D**), whereas dialysis of a scramble peptide (S15, 1.5 mM) had no effect (RS39604/S15, 63 ± 8% of baseline, n = 5, $p < 0.05$; **Figure 2D**). Furthermore, variance analysis of synaptic responses indicates that t-LTD upon chemogenetic inhibition of 5-HT release (**Figure 1**) or application of 5-HT4R antagonists (**Figure 2**) was not accompanied by changes in trial-to-trial variation in EPSP

amplitude (**Figure S3D)**. This further supports a postsynaptic locus of plasticity expression (Shen et al., 2008).

Overall, these data indicate that 5-HT controls plasticity induction in dSPNs through the activation of 5-HT4R, as antagonizing this receptor subtype is sufficient to gate a form of t-LTD. This effect is not mediated by eCBs and relies on postsynaptic expression mechanisms.

Serotonin modulates bAP-induced Ca^{2+} transients during STDP

At glutamatergic synapses on SPNs, the induction of t-LTD depends on the temporal convergence of synaptic input and postsynaptic elevations of dendritic Ca^{2+} signal triggered by back propagating action potentials (bAPs) (Plotkin et al., 2013; Shindou et al., 2011). 5-HT has been shown to regulate ionic conductances that may affect the propagation of bAPs (King et al., 2008). Modulation of the bAP-induced Ca^{2+} signal may therefore be one of the mechanisms that underlies the action of 5-HT at striatal circuits. This may also affect timing-dependent synaptic plasticity in dSPNs (Plotkin et al., 2013; Shindou et al., 2011; Zhou et al., 2005). To test this hypothesis, we performed simultaneous two-photon Ca^{2+} imaging and whole-cell current clamp recordings, and monitored changes in evoked intracellular Ca^{2+} elevations upon the chemogenetic and pharmacological inhibition of 5-HT signaling. In the proximal dendrites of dSPNs, a single bout of the negative STDP protocol (1b-STDP) triggered Ca^{2+} transients that were stable over time, as indicated by the area under the curve of the fluorescence transients not significantly varying over 10 to 15 min (106 ± 8% of control; n = 8, $p > 0.05$; **Figure 3A**). In the dSPNs of $hM4Di^{+/-}/Pet1_{210}$-Cre mice, bath application of CNO (5 μM), thereby impeding 5-HT release, enhanced dendritic Ca^{2+} influx in response to 1b-STDP (Area, 130 ± 8% of control; n = 11, $p < 0.01$; **Figure 3B**). The 1b-STDP-associated dendritic Ca^{2+} signal comparably increased upon application of the two 5-HT4R antagonists GR113808 (5 μM; Area, 122 ± 6% of control; n = 15, $p < 0.01$; **Figure 3C**) or RS39604 (5 μM; Area, 130 ± 7% of control; n = 14, $p < 0.01$; **Figure 3C**).

These results apparently conflict with the notion that typically activation, not inhibition, of Gs-coupled receptors increases Ca^{2+} influx triggered by APs. This increase is through stimulation of protein kinase A (PKA), which enhances voltage gated Ca^{2+} currents (Higley and Sabatini, 2010). Thus, we hypothesized that 5-HT4R regulates dendritic Ca^{2+} levels by influencing the activity of K^+ channels instead. Previous studies in several neuronal subtypes, including striatal SPNs, demonstrate that inhibition of various types of K^+ currents that contribute to the AP repolarization, and after hyperpolarization phases, enhances dendritic Ca^{2+} transients (Cai et al., 2004; Day et al., 2008; Trusel et al., 2015). In addition to PKA, 5-HT4R can also potentially signal to Ca^{2+}/calmodulin-dependent protein kinase II (CaMKII) (Liu and Voyno-Yasenetskaya, 2005; Ponimaskin et al., 2002), which positively regulates the activity of the large-conductance Ca^{2+}-activated K^+ channel BK (Nelson et al., 2005). BK channels shape the duration of bAP in several neuronal populations, and affect dendritic Ca^{2+} influx (Golding et al., 1999). Therefore, reduced release of 5-HT or direct inhibition of 5-HT4R could dampen the activation of BK channels during the STDP protocol, leading to an enhanced dendritic Ca^{2+} signal in response to bAPs. To test this, we first assessed whether blocking BK channels occluded the effect of the 5-HT4R antagonist RS39604. Bath perfusion of the BK channel blocker paxilline (10 μM) significantly enhanced the 1b-STDP-associated Ca^{2+} transient (Area, 138 ± 7% of control; $n = 9$, $p < 0.01$; **Figure 3D**). As predicted, sequential co-application of paxilline with RS39604 had no further effect on the evoked change in dendritic fluorescence (Area, 139 ± 7 % of control; $p < 0.01$; 100 ± 3% of paxilline, $p > 0.05$; $n = 9$; **Figure 3D**), suggesting that BK channels are targets of 5-HT4R signaling.

Our 1b-STDP-stimulation protocol is likely to activate a set of glutamatergic, dopaminergic and serotonergic inputs. Thus, it cannot isolate the impact of 5-HT4R on dendritic Ca^{2+} influx specifically evoked by bAPs. To overcome this issue, we estimated the Ca^{2+} transients generated by somatically eliciting postsynaptic bAPs in the absence of presynaptic stimulation (**Figure 3E**). We replaced the contribution of 5-HT released upon local electrical stimulation with the direct pharmacological stimulation of the 5-HT4R by the agonist RS67333 (5 μM). Consistent with the

hypothesis that 5-HT4R stimulates a K^+ channel conductance, the presence of RS67333 reduced the bAP-induced Ca^{2+} signal (Area, 71 ± 7% of control; n = 10, $p < 0.01$; **Figure 3E**). Furthermore, blocking BK-mediated current prevented the effect of 5-HT4R stimulation. Indeed, RS67333 failed to reduce the bAP-induced Ca^{2+} transients upon pre-exposure to paxilline (Area, paxilline, 142 ± 10% of control; $p < 0.01$; paxilline + RS67333, 142 ± 9% of control, $p < 0.01$; 101 ± 7% of paxilline, $p > 0.05$; n = 7; **Figure 3F**). Further, the intracellular application in the postsynaptic neuron of Autocamtide-2-Related Inhibitory Peptide (AIP, 10 μM), a specific competitive inhibitor of CaMKII, prevented RS6733 from reducing Ca^{2+} transients elicited by bAPs (Area, 105 ± 5% of AIP, $p > 0.05$; n = 10; **Figure 3G**). This indicates that the modulatory effect of 5-HT4R activation is mediated by the CaMKII signaling pathway.

Together, these data indicate that regulation of BK channel activity is required for the 5-HT4R-mediated modulation of dendritic Ca^{2+} signal in dSPNs.

5-HT signaling controls t-LTD at thalamic inputs

We have demonstrated that 5-HT signaling, through the 5-HT4R subtype, influences the postsynaptic response of dSPNs to glutamatergic input activation during STDP. To dissect whether this modulation occurs specifically at cortical and/or thalamic inputs, we interrogated striatal circuitry with optogenetics. We used Thy1-ChR2 transgenic mice to measure postsynaptic responses evoked by light-activation of corticostriatal afferents, which represent the vast majority of excitatory synapses on SPNs (Bolam et al., 2000). In these mice, the expression of channelrhodopsin (ChR2) is high in cortical layer V neurons (**Figure 4A**), and appears not to extend to thalamostriatal neurons (Plotkin et al., 2014; Wu et al., 2015). Short blue light pulses through the microscope objective (0.1-1 ms at 470 nm) elicited excitatory postsynaptic potentials in dSPNs (o-$EPSP_{Ctx}$). We investigated post-pre STDP at corticostriatal synapses by monitoring o-$EPSP_{Ctx}$ before and after the induction protocol. During the post-pre pairing paradigm, optogenetic stimulation of cortical inputs was replaced by conventional electrical stimulation in order to likely

recruit 5-HT fibers (**Figure 4B**). In this experimental setting, the STDP protocol failed to induce significant changes in o-EPSP$_{Ctx}$ (98 ± 8% of baseline, n = 7, p > 0.05; **Figure 4C**), even when applied in the presence of the 5HT4R antagonist RS39604 (5μM; 92 ± 6% of baseline, n = 8, p > 0.05; **Figure 4C**). Thus, corticostriatal synapses to dSPNs are not the primary substrate of the 5-HT4R-mediated effects that we observed at non-dissected glutamatergic inputs (**Figure 2A**). These results also suggest that t-LTD gated upon decreased 5-HT signaling is in fact occurring at thalamostriatal inputs. To test this, we injected either naïve C57BL6J or hM4Di$^{+/-}$/Pet1$_{210}$-Cre mice with the rAAV5-CaMKIIa-ChR2(H134R)-eYFP virus. We targeted the parafascicular (Pf)/central medial (CM) regions of the intralaminar thalamus that project to the DLS (**Figure 4D**) (Ellender et al., 2013), and measured light-evoked EPSPs (o-EPSP$_{Thal}$) at thalamostriatal connections on dSPNs. To induce plasticity, we applied the same post-pre STDP paradigm as for corticostriatal synapses (**Figure 4B** and **4D**). As predicted, the STDP protocol did not evoke plasticity of o-EPSP$_{Thal}$ under control conditions (103 ± 10 % of baseline, n = 6, p > 0.05; **Figure 4E**), whereas it triggered a significant t-LTD of o-EPSP$_{Thal}$ in the presence of RS39604 (5μM; 71 ± 8% of baseline, n = 8, p < 0.05, **Figure 4E**). We then tested the assumption that t-LTD at thalamo-dSPN synapses is attenuated by neuromodulators (including 5-HT) released upon conventional electrical stimulation during STDP, as previously shown at non-dissected glutamatergic inputs (Shen et al., 2015; Wu et al., 2015). For this purpose, we re-examined plasticity of o-EPSP$_{Thal}$ upon the delivery of an optogenetic post-pre pairing STDP protocol (o-STDP), which engages exclusively thalamic afferents. In this experimental setting, we observed a form of t-LTD at thalamo-dSPN synapses (72 ± 6 % of baseline, n = 6, p < 0.05, **Figure S4A**), consistent with previous observations (Wu et al., 2015). Finally, we assessed the link between the synaptic effects of 5-HT at thalamic inputs with the regulation of BK channel activity (**Figure 3**). In our model, decreased 5-HT signaling dampens the activation of BK channels during STDP and boosts the Ca^{2+} signal evoked by bAP (**Figure 3**). This mechanism could underlie the permissive role of 5-HT4R inhibition on t-LTD induction (**Figure 2A** and **Figure 4E**). If this is the case, we would expect the pharmacological inhibition of

BK channels during conventional STDP (**Figure S4B**) to be sufficient to gate synaptic depression at thalamic inputs. Reminiscent of 5-HT4R antagonism or chemogenetic inhibition of 5-HT release, in the presence of the BK channel blocker paxilline (10 μM), the STDP paradigm resulted in t-LTD of o-EPSP$_{Thal}$ (75 ± 4 % of baseline, n = 7, $p < 0.05$, **Figure S4B**).

hM4Di$^{+/-}$/Pet1$_{210}$-Cre animals showed similar effects (**Figure 4F**). The chemogenetic inhibition of 5-HT release by bath application of CNO (5 μM) during the post-pre STDP paradigm enabled t-LTD at thalamostriatal synapses (dSPN$_{DREADD_Thal,}$ 93 ± 1 % of baseline, n = 7, $p > 0.05$; dSPN$_{DREADD_Thal,}$ + CNO, 61 ± 5 % of baseline, n = 7, $p < 0.05$; **Figure 4F**).

In summary, our findings support the conclusion that 5-HT signaling controls t-LTD at thalamic synapses on dSPNs. These synaptic effects of 5-HT are mediated by the 5-HT4R subtype, which shapes bAP-evoked dendritic Ca^{2+} signals through the regulation of BK channel activity.

Discussion

The results presented here reveal a previously unknown role of 5-HT at striatal circuits. This is the first demonstration that signaling by 5-HT receptors provides a control mechanism of Hebbian plasticity at SPN synapses of the direct pathway. Previous observations showed that increasing 5-HT levels in the DLS reduces presynaptic glutamate release and depresses neurotransmission at corticostriatal inputs (Mathur et al., 2011). We find that impeding serotonergic signaling, thereby dampening the activation of the 5-HT4R subtype, affects postsynaptic dendritic Ca^{2+} signals and gates spike-timing-dependent long-term depression (t-LTD) preferentially at thalamic afferents. Although DRN terminals have been shown to co-release 5-HT and glutamate (Liu et al., 2014), the evidence that pharmacological inhibition of 5-HT4R fully recapitulates the effects of chemogenetic inhibition of striatal DRN afferents supports the specific contribution of 5-HT in the observed phenomena.

Our findings add to the very limited knowledge of the intracellular signaling pathways regulating the thalamostriatal system, and in particular the molecular mechanisms underlying synaptic depression of thalamo-dSPN synapses (Atwood et al., 2014; Parker et al., 2016; Wu et al., 2015). Spike-timing-dependent LTD (t-LTD) at thalamostriatal inputs has been shown to be independent of eCBs released from the postsynaptic SPN (Wu et al., 2015). Consistent with this and with the evidence that thalamic afferents to the striatum are devoid of presynaptic CB1R (Wu et al., 2015), we find that t-LTD gated by 5-HT4R antagonism is insensitive to CB1R inhibition, and relies on postsynaptic expression mechanisms. In the DS, 5-HT4Rs are localized mainly post-synaptically (Di Matteo et al., 2008). Activation of this Gs-coupled receptor subtype typically increases PKA activity and leads to the inhibition of K^+ channels (King et al., 2008). Our findings point to an alternative signaling mechanism, which involves protein CaMKII and activation of large-conductance BK channels. Indeed, 5-HT4R can couple not only with Gs proteins, but also with Gα13, which signals to CaMKII (Liu and Voyno-Yasenetskaya, 2005; Nelson et al., 2005; Ponimaskin et al., 2002). In brain regions other than the striatum, CaMKII positively regulates BK

channels (Nelson et al., 2005; Smith et al., 2002). We propose a model in which 5-HT, by modulating the activity of BK channels, controls the dendritic Ca^{2+} signal and influences spike-timing–dependent plasticity. In this view, low 5-HT levels associated with behavioral states or pathology would result in dampened activation of BK channels and enhanced Ca^{2+} signal evoked by bAP; this may facilitate the Ca^{2+}-dependent internalization of AMPAR, enabling LTD (Luscher et al., 2000). Supporting this model, t-LTD gated by 5-HT4R antagonism at non-dissected glutamatergic inputs to dSPN is blocked upon disruption of the interaction between dynamin and amphiphysin, which is crucial for AMPAR endocytosis (Morishita et al., 2005). Furthermore, the pharmacological inhibition of BK channel activity, which boosts bAP-evoked Ca^{2+} elevations during STDP and interferes with the 5-HT4R-mediated modulation of intracellular Ca^{2+} transients, is sufficient to gate t-LTD at thalamostriatal afferents.

The 5-HT-mediated regulation of dendritic Ca^{2+} signal during timing-dependent plasticity represents a novel neuromodulatory means by which changes in serotonergic levels may shape the thalamostriatal system. Thalamostriatal projections are thought to convey salient sensory stimuli (Bradfield et al., 2013; Matsumoto et al., 2001). It has been proposed that projections of the intralaminar nuclei of the thalamus to the striatum, and interaction with local circuit elements, are critical to interrupt ongoing motor behavior and redirect attention toward salient stimuli (Thorn and Graybiel, 2010). Therefore, gating mechanisms of LTD at thalamic inputs that depend on serotonergic levels may affect the BG network and striatal-information processing. Although our findings cannot establish the precise identity of the intralaminar thalamic afferents that are modulated by 5-HT, only thalamic inputs from the Pf nucleus, and not from the CL nucleus, have been shown to express LTD (Ellender et al., 2013).

Our results indicate that 5-HT at thalamic inputs, through 5-HT4R, exerts a similar function to DA at cortical inputs though D1R (Shen et al., 2008); both signaling pathways contribute to the activation of dSPNs by increasing the strength of glutamatergic inputs. The fact that the activation of D1R by DA released during intrastriatal stimulation (Shen et al., 2015; Threlfell et al., 2012; Wu

et al., 2015) cannot compensate for the decrease in Gs signaling when 5-HT4R is blocked suggests that D1R and 5-HT4R may not be localized in the same functional microdomain. Further studies are needed to assess whether D1Rs segregate at cortical spines and 5-HT4Rs at thalamic ones, or whether the input-specific effects of 5-HT signaling require cross-talk with a presynaptic element specific for thalamo-striatal synapses.

In the ventral striatum, DA supports reinforcement learning by acting in a critical time window after the sensorimotor signal (Yagishita et al., 2014). This process, which requires activation of PKA in the dendritic spines of dSPNs, is independent of Ca^{2+} influx triggered by bAPs, and results in dendritic spine enlargement and synaptic potentiation in response to a STDP paradigm. Although it is unknown whether similar D1-mediated effects occur in dSPNs of the DS, it is tempting to speculate that DA and 5-HT may act through different subcellular mechanisms – the first involving spine plasticity and the second shaping bAP evoked dendritic Ca^{2+} signal – to encode reward stimuli at the cellular level. Building on existing models of striatal plasticity, we may now recognize excitatory DA and 5-HT as two complementary neuromodulatory systems, controlling timing-dependent plasticity at two different glutamatergic inputs to dSPNs. This might allow for greater selectivity in tuning the activity of the direct pathway, which supports reinforcement and reward (Kravitz et al., 2012).

Overall, the findings from our studies not only provide new mechanistic insights on the thalamic control of striatal functions, but also identify novel synaptic substrates for maladaptive plasticity in BG disorders that involve dysfunction of the serotonergic system.

Experimental procedures

All procedures involving animals were carried out in accordance with the Italian Ministry of Health's directives (D.lgs 26/2014) regulating animal research.

Generation of the hM4Di conditional knock-in mouse line

Detailed methods for the generation of hM4Di conditional knock-in mouse line are provided in the **Supplemental Experimental Procedures.**

Surgeries

Five- to six-week-old mice were anesthetized and placed in a stereotaxic frame, and a glass capillary was inserted for viral injections into the intalaminar thalamus (-2.3 AP; ±0.75 ML; -3.5 DV). A volume of 0.5 μl/site of virus was injected at a rate of 0.1 μl/min.

Electrophysiology

Current-clamp recordings were made from direct pathway striatal projection neurons (dSPNs) of the dorsolateral striatum (DLS) or from serotonergic neurons of the dorsal raphe nucleus (DRN). In the DLS, excitatory postsynaptic potentials (EPSPs) were evoked at 0.05 Hz by intrastriatal electrical stimulation using a concentric bipolar electrode (20-80 μA; 40-60 μs; FHC, Bowdoin, Maine), or by optogenetic stimulation of cortical or thalamic afferents using short blue light pulses (470 nm, 0.1-1 ms) of LED light (coolLED, pE100, Andover, Hampshire, United Kingdom) delivered through the microscope objective (40X). STDP was induced as described (Nazzaro et al., 2012); see also **Supplemental Experimental Procedures**.

Imaging

Ca^{2+} transients were imaged with 100 µM Fluo-4 (Life Technologies, Carlsbad, California). Alexa 568 (10 µM, Invitrogen, Carlsbad, California) was used for visualization of cell bodies and dendrites. Two-photon Ca^{2+} imaging was performed with a Leica SP5 AOBS upright DM6000 CFS microscope coupled with a 2P laser Chameleon Ultra Coherent (800 nm light pulsed at 90 MHz; pulse duration: ≈250 fs), and equipped with a Leica 25x NA 0.95 water-immersion objective. Fluorescence line-scan signals were acquired every 6 ms and 256 pixels per line, with 0.1 µm pixels and 20 µs pixel dwell time. Images were collected with LAS AF Leica software and analyzed using ImageJ software (version 1.45, http://rsb.info.nih.gov/ij/, NIH, Maryland) and Origin 9.1 (OriginLab Corporation, Northampton, Massachussets). For data analysis, transients were digitally filtered off-line (adjacent-averaging routine, smoothing factor n = 5; Origin 9.1); see also **Supplemental Experimental Procedures**.

Immunostaining

Identification of dSPNs

During electrophysiology experiments, SPNs were filled with Neurobiotin (0.5 mg/ml) and slices were subsequently fixed with 4% paraformaldehyde (PFA) in phosphate buffer (PB). Antigen retrieval was performed, and the slices were incubated in primary antibodies (anti-A2A, 1:250, Enzo Life Sciences, Farmingdale, New York; and anti-substance P, 1:200, Millipore, Billerica, Massachussets) (Trusel et al., 2015). Sections were then incubated in Alexa 568-conjugated streptavidin (1:1000; Invitrogen, Carlsbad, California), followed by secondary antibodies (Invitrogen, Carlsbad, California); see also **Supplemental Experimental Procedures**.

Immunofluorescence

Mice were perfused with 4% PFA in phosphate buffer (PB) and vibratome sections (50 µm) were processed for immunofluorescence (Migliarini et al., 2013); see also **Supplemental Experimental Procedures**.

Immuno EM analysis

The immuno-EM analyses were performed as described (Hebert-Chatelain et al., 2014); see also **Supplemental Experimental Procedures**.

Data Analysis

The occurrence and magnitude of synaptic plasticity was evaluated by comparing the normalized EPSP amplitudes from the last 5 min of baseline recordings with the corresponding values at 25-35 min after STDP. LTD plots were generated by averaging the peak amplitude of individual EPSPs in 1 min bins. Coefficient of variation (CV) for EPSP was calculated by the ratio of the standard deviation (sd) and the mean EPSP amplitude (Shen et al., 2008). In imaging experiments, the magnitude of the Ca^{2+} signal was measured as the area under the curve in the transient region.

Statistics

Electrophysiological data were analyzed by one-way repeated measures ANOVA (RM1W) for comparisons within a group, and by one-way ANOVA (1W) for between-group comparisons (GraphPad Prism 6 software). *Post-hoc* analysis (Tukey) was performed only when ANOVA yielded a significant main effect. Two groups were tested for statistical significance using the Mann Whitney U-nonparametric test (GraphPad Prism 6 software). Calcium imaging data were analyzed by the independent two-population t test (GraphPad Prism 6 software).

Author contributions

M.G. designed and performed the electrophysiological and imaging experiments A.G., M.P., A.G. designed and generated the hM4Di$^{+/-}$/Pet1$_{210}$-Cre mouse line. A.C. designed and conducted some electrophysiological recordings. M.G., A.G. and M.T made intracerebral virus injections. M.T. and M.G. performed the immunostaining for the identification of dSPNs and S.M. carried out the immunofluorescence analysis. T.C. and R.M. performed the electron microscopy analysis. M.G., A.C., M.T. and M.P contributed to critical reading of the manuscript. R.T. supervised the project, directed the experiments, and wrote the manuscript.

Acknowledgments

We are grateful to Mattia Pesce for technical assistance during imaging experiments. This research was supported by the Fondazione Istituto Italiano di Tecnologia, and by grants provided by Compagnia di San Paolo (to RT) and Fondazione Cariplo (to RT).

Competing financial interests

The authors declare no competing financial interests.

References

Atwood, B.K., Kupferschmidt, D.A., and Lovinger, D.M. (2014). Opioids induce dissociable forms of long-term depression of excitatory inputs to the dorsal striatum. Nature neuroscience *17*, 540-548.

Bateup, H.S., Santini, E., Shen, W., Birnbaum, S., Valjent, E., Surmeier, D.J., Fisone, G., Nestler, E.J., and Greengard, P. (2010). Distinct subclasses of medium spiny neurons differentially regulate striatal motor behaviors. Proc Natl Acad Sci U S A *107*, 14845-14850.

Bolam, J.P., Hanley, J.J., Booth, P.A., and Bevan, M.D. (2000). Synaptic organisation of the basal ganglia. J Anat *196 (Pt 4)*, 527-542.

Bradfield, L.A., Hart, G., and Balleine, B.W. (2013). The role of the anterior, mediodorsal, and parafascicular thalamus in instrumental conditioning. Frontiers in systems neuroscience *7*, 51.

Cai, X., Liang, C.W., Muralidharan, S., Kao, J.P., Tang, C.M., and Thompson, S.M. (2004). Unique roles of SK and Kv4.2 potassium channels in dendritic integration. Neuron *44*, 351-364.

Carroll, R.C., Beattie, E.C., Xia, H., Luscher, C., Altschuler, Y., Nicoll, R.A., Malenka, R.C., and von Zastrow, M. (1999a). Dynamin-dependent endocytosis of ionotropic glutamate receptors. Proc Natl Acad Sci U S A *96*, 14112-14117.

Carroll, R.C., Lissin, D.V., von Zastrow, M., Nicoll, R.A., and Malenka, R.C. (1999b). Rapid redistribution of glutamate receptors contributes to long-term depression in hippocampal cultures. Nature neuroscience *2*, 454-460.

Day, M., Wokosin, D., Plotkin, J.L., Tian, X., and Surmeier, D.J. (2008). Differential excitability and modulation of striatal medium spiny neuron dendrites. J Neurosci *28*, 11603-11614.

Di Matteo, V., Pierucci, M., Esposito, E., Crescimanno, G., Benigno, A., and Di Giovanni, G. (2008). Serotonin modulation of the basal ganglia circuitry: therapeutic implication for Parkinson's disease and other motor disorders. Prog Brain Res *172*, 423-463.

Ellender, T.J., Harwood, J., Kosillo, P., Capogna, M., and Bolam, J.P. (2013). Heterogeneous properties of central lateral and parafascicular thalamic synapses in the striatum. J Physiol *591*, 257-272.

Eskenazi, D., Brodsky, M., and Neumaier, J.F. (2015). Deconstructing 5-HT6 receptor effects on striatal circuit function. Neuroscience *299*, 97-106.

Fornal, C.A., Metzler, C.W., Marrosu, F., Ribiero-do-Valle, L.E., and Jacobs, B.L. (1996). A subgroup of dorsal raphe serotonergic neurons in the cat is strongly activated during oral-buccal movements. Brain Res *716*, 123-133.

Gerfen, C.R., and Surmeier, D.J. (2011). Modulation of striatal projection systems by dopamine. Annu Rev Neurosci *34*, 441-466.

Goddard, A.W., Shekhar, A., Whiteman, A.F., and McDougle, C.J. (2008). Serotoninergic mechanisms in the treatment of obsessive-compulsive disorder. Drug Discov Today *13*, 325-332.

Golding, N.L., Jung, H.Y., Mickus, T., and Spruston, N. (1999). Dendritic calcium spike initiation and repolarization are controlled by distinct potassium channel subtypes in CA1 pyramidal neurons. J Neurosci *19*, 8789-8798.

Hannon, J., and Hoyer, D. (2008). Molecular biology of 5-HT receptors. Behav Brain Res *195*, 198-213.

Hebert-Chatelain, E., Reguero, L., Puente, N., Lutz, B., Chaouloff, F., Rossignol, R., Piazza, P.V., Benard, G., Grandes, P., and Marsicano, G. (2014). Cannabinoid control of brain bioenergetics: Exploring the subcellular localization of the CB1 receptor. Mol Metab *3*, 495-504.

Higley, M.J., and Sabatini, B.L. (2010). Competitive regulation of synaptic Ca2+ influx by D2 dopamine and A2A adenosine receptors. Nature neuroscience *13*, 958-966.

Jacobs, B.L., and Fornal, C.A. (1999). Activity of serotonergic neurons in behaving animals. Neuropsychopharmacology *21*, 9S-15S.

King, M.V., Marsden, C.A., and Fone, K.C. (2008). A role for the 5-HT(1A), 5-HT4 and 5-HT6 receptors in learning and memory. Trends Pharmacol Sci *29*, 482-492.

Kravitz, A.V., Freeze, B.S., Parker, P.R., Kay, K., Thwin, M.T., Deisseroth, K., and Kreitzer, A.C. (2010). Regulation of parkinsonian motor behaviours by optogenetic control of basal ganglia circuitry. Nature *466*, 622-626.

Kravitz, A.V., Tye, L.D., and Kreitzer, A.C. (2012). Distinct roles for direct and indirect pathway striatal neurons in reinforcement. Nature neuroscience *15*, 816-818.

Kreitzer, A.C., and Malenka, R.C. (2007). Endocannabinoid-mediated rescue of striatal LTD and motor deficits in Parkinson's disease models. Nature *445*, 643-647.

Liu, G., and Voyno-Yasenetskaya, T.A. (2005). Radixin stimulates Rac1 and Ca2+/calmodulin-dependent kinase, CaMKII: cross-talk with Galpha13 signaling. J Biol Chem *280*, 39042-39049.

Liu, Z., Zhou, J., Li, Y., Hu, F., Lu, Y., Ma, M., Feng, Q., Zhang, J.E., Wang, D., Zeng, J.*, et al.* (2014). Dorsal raphe neurons signal reward through 5-HT and glutamate. Neuron *81*, 1360-1374.

Luscher, C., Nicoll, R.A., Malenka, R.C., and Muller, D. (2000). Synaptic plasticity and dynamic modulation of the postsynaptic membrane. Nature neuroscience *3*, 545-550.

Mathur, B.N., Capik, N.A., Alvarez, V.A., and Lovinger, D.M. (2011). Serotonin induces long-term depression at corticostriatal synapses. J Neurosci *31*, 7402-7411.

Mathur, B.N., and Lovinger, D.M. (2012). Serotonergic action on dorsal striatal function. Parkinsonism Relat Disord *18 Suppl 1*, S129-131.

Matsumoto, N., Minamimoto, T., Graybiel, A.M., and Kimura, M. (2001). Neurons in the thalamic CM-Pf complex supply striatal neurons with information about behaviorally significant sensory events. J Neurophysiol *85*, 960-976.

Migliarini, S., Pacini, G., Pelosi, B., Lunardi, G., and Pasqualetti, M. (2013). Lack of brain serotonin affects postnatal development and serotonergic neuronal circuitry formation. Mol Psychiatry *18*, 1106-1118.

Morishita, W., Marie, H., and Malenka, R.C. (2005). Distinct triggering and expression mechanisms underlie LTD of AMPA and NMDA synaptic responses. Nature neuroscience *8*, 1043-1050.

Navailles, S., and De Deurwaerdere, P. (2011). Presynaptic control of serotonin on striatal dopamine function. Psychopharmacology (Berl) *213*, 213-242.

Nazzaro, C., Greco, B., Cerovic, M., Baxter, P., Rubino, T., Trusel, M., Parolaro, D., Tkatch, T., Benfenati, F., Pedarzani, P.*, et al.* (2012). SK channel modulation rescues striatal plasticity and control over habit in cannabinoid tolerance. Nature neuroscience.

Nelson, A.B., Gittis, A.H., and du Lac, S. (2005). Decreases in CaMKII activity trigger persistent potentiation of intrinsic excitability in spontaneously firing vestibular nucleus neurons. Neuron *46*, 623-631.

O'Hare, J.K., Ade, K.K., Sukharnikova, T., Van Hooser, S.D., Palmeri, M.L., Yin, H.H., and Calakos, N. (2016). Pathway-Specific Striatal Substrates for Habitual Behavior. Neuron *89*, 472-479.

Parker, P.R., Lalive, A.L., and Kreitzer, A.C. (2016). Pathway-Specific Remodeling of Thalamostriatal Synapses in Parkinsonian Mice. Neuron *89*, 734-740.

Pelosi, B., Migliarini, S., Pacini, G., Pratelli, M., and Pasqualetti, M. (2014). Generation of Pet1210-Cre transgenic mouse line reveals non-serotonergic expression domains of Pet1 both in CNS and periphery. PLoS One *9*, e104318.

Plotkin, J.L., Day, M., Peterson, J.D., Xie, Z., Kress, G.J., Rafalovich, I., Kondapalli, J., Gertler, T.S., Flajolet, M., Greengard, P.*, et al.* (2014). Impaired TrkB receptor signaling underlies corticostriatal dysfunction in Huntington's disease. Neuron *83*, 178-188.

Plotkin, J.L., Shen, W., Rafalovich, I., Sebel, L.E., Day, M., Chan, C.S., and Surmeier, D.J. (2013). Regulation of dendritic calcium release in striatal spiny projection neurons. J Neurophysiol *110*, 2325-2336.

Ponimaskin, E.G., Profirovic, J., Vaiskunaite, R., Richter, D.W., and Voyno-Yasenetskaya, T.A. (2002). 5-Hydroxytryptamine 4(a) receptor is coupled to the Galpha subunit of heterotrimeric G13 protein. J Biol Chem *277*, 20812-20819.

Shen, W., Flajolet, M., Greengard, P., and Surmeier, D.J. (2008). Dichotomous dopaminergic control of striatal synaptic plasticity. Science *321*, 848-851.

Shen, W., Plotkin, J.L., Francardo, V., Ko, W.K., Xie, Z., Li, Q., Fieblinger, T., Wess, J., Neubig, R.R., Lindsley, C.W., *et al.* (2015). M4 Muscarinic Receptor Signaling Ameliorates Striatal Plasticity Deficits in Models of L-DOPA-Induced Dyskinesia. Neuron *88*, 762-773.

Shindou, T., Ochi-Shindou, M., and Wickens, J.R. (2011). A Ca(2+) threshold for induction of spike-timing-dependent depression in the mouse striatum. J Neurosci *31*, 13015-13022.

Sippy, T., Lapray, D., Crochet, S., and Petersen, C.C. (2015). Cell-Type-Specific Sensorimotor Processing in Striatal Projection Neurons during Goal-Directed Behavior. Neuron *88*, 298-305.

Smith, M.R., Nelson, A.B., and Du Lac, S. (2002). Regulation of firing response gain by calcium-dependent mechanisms in vestibular nucleus neurons. J Neurophysiol *87*, 2031-2042.

Tecuapetla, F., Jin, X., Lima, S.Q., and Costa, R.M. (2016). Complementary Contributions of Striatal Projection Pathways to Action Initiation and Execution. Cell *166*, 703-715.

Thorn, C.A., and Graybiel, A.M. (2010). Pausing to regroup: thalamic gating of cortico-basal ganglia networks. Neuron *67*, 175-178.

Threlfell, S., Lalic, T., Platt, N.J., Jennings, K.A., Deisseroth, K., and Cragg, S.J. (2012). Striatal dopamine release is triggered by synchronized activity in cholinergic interneurons. Neuron *75*, 58-64.

Tritsch, N.X., Ding, J.B., and Sabatini, B.L. (2012). Dopaminergic neurons inhibit striatal output through non-canonical release of GABA. Nature *490*, 262-266.

Trusel, M., Cavaccini, A., Gritti, M., Greco, B., Saintot, P.P., Nazzaro, C., Cerovic, M., Morella, I., Brambilla, R., and Tonini, R. (2015). Coordinated Regulation of Synaptic Plasticity at Striatopallidal and Striatonigral Neurons Orchestrates Motor Control. Cell Rep *13*, 1353-1365.

Vicente, A.M., Galvao-Ferreira, P., Tecuapetla, F., and Costa, R.M. (2016). Direct and indirect dorsolateral striatum pathways reinforce different action strategies. Curr Biol *26*, R267-269.

Vilaro, M.T., Cortes, R., Gerald, C., Branchek, T.A., Palacios, J.M., and Mengod, G. (1996). Localization of 5-HT4 receptor mRNA in rat brain by in situ hybridization histochemistry. Brain Res Mol Brain Res *43*, 356-360.

Wu, Y.W., Kim, J.I., Tawfik, V.L., Lalchandani, R.R., Scherrer, G., and Ding, J.B. (2015). Input- and Cell-Type-Specific Endocannabinoid-Dependent LTD in the Striatum. Cell Rep *10*, 75-87.

Yagishita, S., Hayashi-Takagi, A., Ellis-Davies, G.C., Urakubo, H., Ishii, S., and Kasai, H. (2014). A critical time window for dopamine actions on the structural plasticity of dendritic spines. Science *345*, 1616-1620.

Zhou, Y.D., Acker, C.D., Netoff, T.I., Sen, K., and White, J.A. (2005). Increasing Ca2+ transients by broadening postsynaptic action potentials enhances timing-dependent synaptic depression. Proc Natl Acad Sci U S A *102*, 19121-19125.

Figure 1

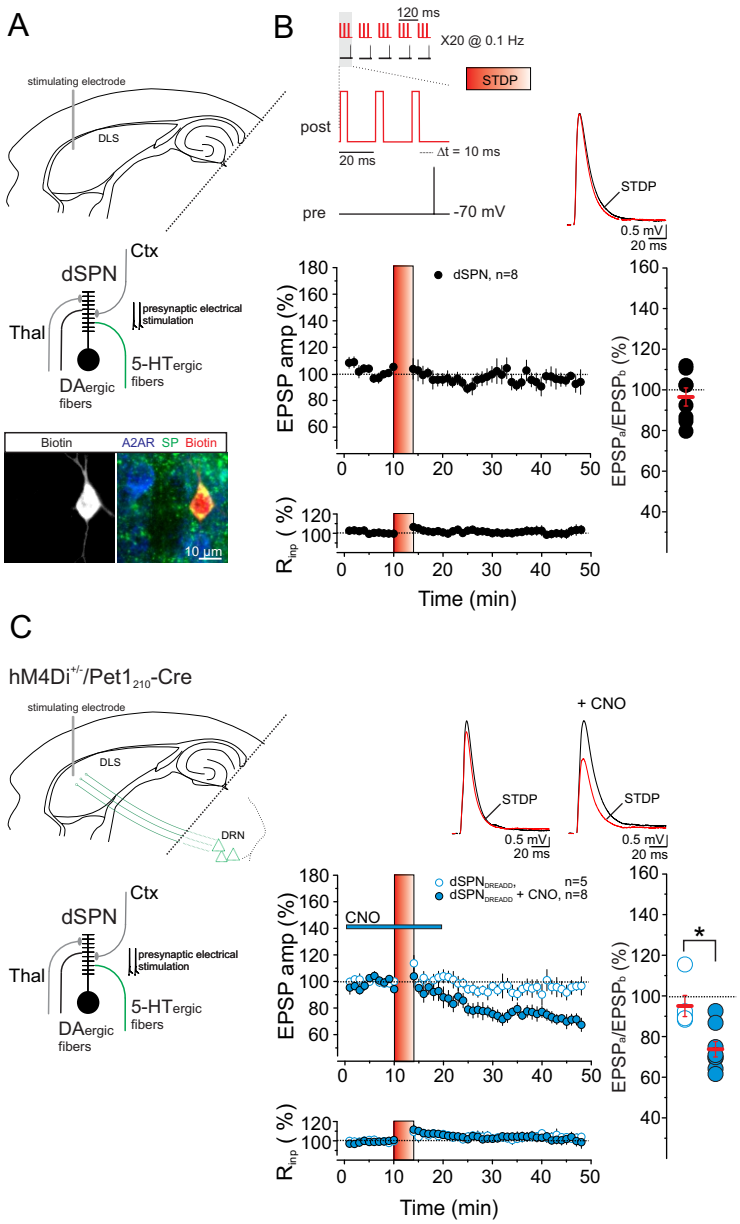
A
stimulating electrode
DLS
Ctx
dSPN
Thal
presynaptic electrical stimulation
5-HTergic fibers
DAergic fibers
Biotin
A2AR SP Biotin
10 µm
B
120 ms
X20 @ 0.1 Hz
STDP
post
20 ms
Δt = 10 ms
pre
-70 mV
STDP
0.5 mV
20 ms
dSPN, n=8
EPSP amp (%)
EPSPa/EPSPb (%)
Rinp (%)
Time (min)
C
hM4Di+/-/Pet1210-Cre
stimulating electrode
DLS
DRN
Ctx
dSPN
Thal
presynaptic electrical stimulation
5-HTergic fibers
DAergic fibers
+ CNO
STDP
STDP
0.5 mV
20 ms
0.5 mV
20 ms
dSPNDREADD, n=5
dSPNDREADD + CNO, n=8
CNO
*
EPSP amp (%)
EPSPa/EPSPb (%)
Rinp (%)
Time (min)

Figure 1. Chemogenetic inhibition of 5-HT release in the DLS promotes the induction of t-LTD at dSPN glutamatergic synapses

(**A**) (Top) Experimental configuration in horizontal brain slices containing the dorsolateral striatum (DLS). Schematic shows glutamatergic cortical and thalamic inputs to dSPNs, as well dopaminergic and serotonergic afferents, which are recruited following intrastriatal electrical stimulation. (Bottom) Confocal laser scanning microscopy images of triple immunofluorescence for adenosine A2A receptor (A2AR), substance P (SP) and biotin in patched recorded neurons.

(**B**) (Top) The post-pre pairing protocol for the induction of t-LTD. (Bottom) In dSPNs from naive mice, t-LTD was not induced by the post-pre timing pairing (dSPN, RM1WA $F_{7,44}$=1, p=0.4).

(**C**) Experimental configuration in brain slices from hM4Di$^{+/-}$/Pet1$_{210}$-Cre mice, highlighting the 5-HT terminals (green) originating from the Dorsal Raphe Nucleus (DRN). In DLS dSPNs from these mice, bath perfusion of CNO (5 μM; blue bar) during STDP gated a form of t-LTD, which was absent under control conditions (dSPN$_{DREADD}$ + CNO, RM1WA $F_{7,44}$=8, p< 0.0001, p< 0.05 Tukey; dSPN$_{DREADD}$, RM1WA $F_{4,44}$=1.5, p=0.3; dSPN$_{DREADD}$ + CNO versus dSPN$_{DREADD}$, * p< 0.05, Mann Whitney test).

(**B**,**C**) Data are presented as time courses (mean ± s.e.m.) of normalized EPSP amplitudes and normalized Rinp. Scatter plot summarizes the ratios of synaptic responses after (a) and before (b) the STDP. Insets represent superimposed averaged recordings (ten traces) before (black line) and after (red line) the delivery of the STDP protocol (red vertical bar).

Figure 2

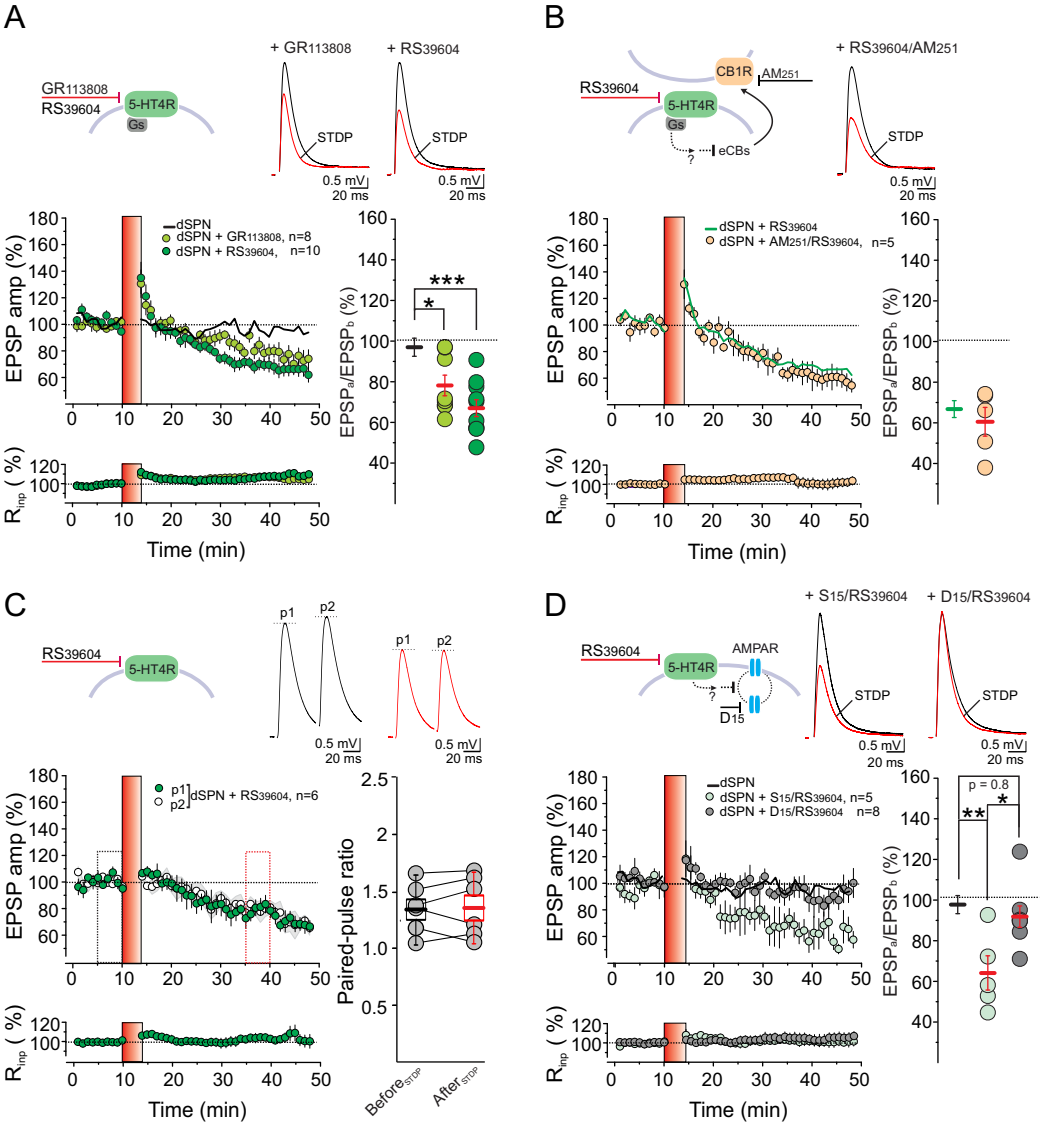
A
+ GR113808
+ RS39604
GR113808
RS39604
5-HT4R
Gs
STDP
0.5 mV
20 ms
dSPN
dSPN + GR113808, n=8
dSPN + RS39604, n=10
EPSP amp (%)
EPSPa/EPSPb (%)
***
*
Rinp (%)
Time (min)
B
+ RS39604/AM251
RS39604
CB1R
AM251
5-HT4R
Gs
eCBs
dSPN + RS39604
dSPN + AM251/RS39604, n=5
C
RS39604
5-HT4R
p1
p2
dSPN + RS39604, n=6
Paired-pulse ratio
Before STDP
After STDP
D
+ S15/RS39604
+ D15/RS39604
AMPAR
D15
dSPN
dSPN + S15/RS39604, n=5
dSPN + D15/RS39604 n=8
p = 0.8
**
*

Figure 2. Antagonizing the 5-HT4R subtype is a permissive condition for t-LTD to occur

(**A**) t-LTD was observed at glutamatergic dSPN synapses when the post-pre STDP protocol was delivered in the presence of the 5-HT4R antagonists GR113808 or RS39604 (5 μM; GR113808, RM1WA $F_{7,44}$=7, p=0.003, p< 0.05 Tukey; RS39604, RM1WA $F_{9,44}$=14, p< 0.0001, p< 0.05 Tukey; 1WA $F_{2,23}$=10, p= 0.0008, dSPN+ GR113808 versus dSPN, *p< 0.05, dSPN+ RS39604 versus dSPN, ***p< 0.001; Tukey). The two 5-HT4R antagonists were applied throughout the entire duration of the recording. Solid black line (average) is the time course from **Figure 1B**, reported here for reference.

(**B**) t-LTD gated by RS39604 was not blocked by the CB1R antagonist AM251 (5 μM; dSPN + RS39604/AM251, RM1WA $F_{4,44}$=10 p= 0.001, p< 0.05 Tukey; dSPN + RS39604/AM251 versus dSPN + RS39604, p=0.6, Mann Whitney test). Solid green line (average) is t-LTD from (**A**) obtained in the presence of RS39604, reported here for reference.

(**C**) t-LTD induced with the post-pre paring upon application of RS39604 (5 μM) is not associated with changes in paired-pulse-ratio (PPR). (Left) Plot shows the normalized first peak (p1) and second peak (p2) amplitudes of synaptic responses generated by twin stimuli at a 50-ms interval as a function of time (dSPN + RS39604: p1, RM1WA $F_{5,44}$=5 p< 0.0001, p< 0.05 Tukey; p2, RM1WA $F_{5,44}$=6 p< 0.0001, p< 0.05 Tukey). (Right) Box-chart diagram indicates the PPRs of baseline (black box), and after STDP (red box) at the time points indicated. The values are the minimum, mean (bar inside the box), and the maximum. PPR was expressed as the ratio between the amplitude of the second and the first EPSPs.

(**D**) t-LTD was blocked by intracellular application of the endocytosis-disrupting peptide D15 (1.5 mM; dSPN + D15, RM1WA $F_{7,44}$=1.7 p= 0.17) but not of the scramble peptide, S15 (1.5 mM; dSPN + S15, RM1WA $F_{4,44}$=4, p= 0.03, p< 0.05 Tukey) (1WA, $F_{2,18}$=8, p= 0.0031; dSPN + D15 versus dSPN, p=0.8, dSPN + D15 versus dSPN + S15, *p< 0.05, dSPN + S15 versus

dSPN, **p< 0.01; Tukey). Solid black line (average) is the time course from **Figure 1B**, reported here for reference.

(**A**-**D**) (Left) Time courses (mean ± s.e.m.) of normalized EPSP amplitudes and normalized Rinp. (Insets, right) Averaged recordings (ten traces) before (black line) and after (red line) the delivery of the STDP protocol (red vertical bar). (Insets, left) Schematic of proposed 5-HTR subtype (**A**,**C**) or signaling pathway (**B,D**) targeted by the defined antagonists. (**A**,**B**,**D**) (Right) Plot of ratios of synaptic responses after (a) and before (b) the STDP.

Figure 3

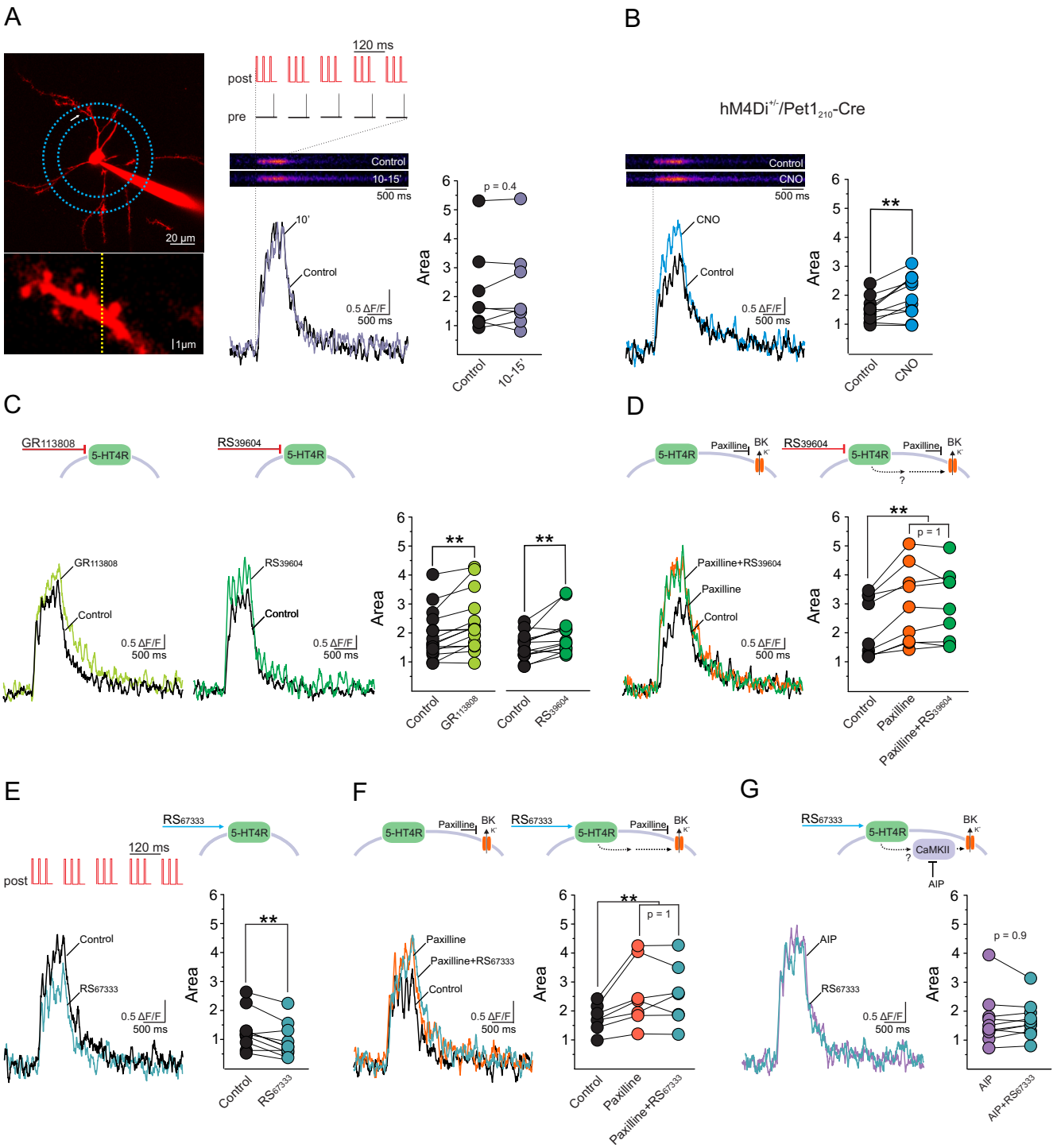
A
20 µm
1µm
120 ms
post
pre
Control
10-15'
500 ms
10'
Control
0.5 ΔF/F
500 ms
p = 0.4
Area
Control
10-15'
B
hM4Di+/-/Pet1210-Cre
Control
CNO
500 ms
CNO
Control
0.5 ΔF/F
500 ms
**
Area
Control
CNO
C
GR113808
5-HT4R
RS39604
5-HT4R
GR113808
Control
0.5 ΔF/F
500 ms
RS39604
Control
0.5 ΔF/F
500 ms
**
**
Area
Control
GR113808
Control
RS39604
D
5-HT4R
Paxilline
BK
RS39604
5-HT4R
Paxilline
BK
?
Paxilline+RS39604
Paxilline
Control
0.5 ΔF/F
500 ms
**
p = 1
Area
Control
Paxilline
Paxilline+RS39604
E
RS67333
5-HT4R
120 ms
post
Control
RS67333
0.5 ΔF/F
500 ms
**
Area
Control
RS67333
F
5-HT4R
Paxilline
BK
RS67333
5-HT4R
Paxilline
BK
Paxilline
Paxilline+RS67333
Control
0.5 ΔF/F
500 ms
**
p = 1
Area
Control
Paxilline
Paxilline+RS67333
G
RS67333
5-HT4R
BK
CaMKII
?
AIP
AIP
RS67333
0.5 ΔF/F
500 ms
p = 0.9
Area
AIP
AIP+RS67333

Figure 3. 5-HT signaling modulates bAP-evoked dendritic Ca^{2+} transients in dSPNs

(**A**) (Top left) Maximum-intensity projection images of a dSPN filled with Alexa 568. Blue dotted circle lines delimit the region of proximal dendrites, 30-50 μm from the soma. (Bottom left) High-magnification of a dSPN proximal dendrite from which line scans were taken (yellow dotted line). (Center) Dendritic Ca^{2+} transients and the corresponding relative changes in fluorescence that are evoked by one bout of the post-pre STDP paradigm (1b-STDP, inset) for control conditions, and after 10 to 15 min (paired t-test, p = 0.4). (**B**) Chemogenetic inhibition of 5-HT release in the DLS of hM4Di$^{+/-}$/Pet1$_{210}$-Cre mice boosts dendritic Ca^{2+} transients in response to 1b-STDP.

(**B-G**) Comparison of Ca^{2+} transients in response to 1b-STDP (**B-D**) or to a burst pattern of bAPs (**E-G**), before and after a specific pharmacological manipulation, as indicated.

(**A-G**) (Right) Plot summary of modulation of evoked dendritic Ca^{2+} elevations measured as area under the curve of the fluorescence transients, in control conditions and with the pharmacological manipulations, as indicated (**A**,**B**,**C**,**E**,**G**, paired t-test, ** p< 0.01; **D**, RM1WA, $F_{8,2}$=20 p< 0.0001, paxilline versus control, p< 0.001, Tukey; paxilline + RS39604 versus control, p< 0.001, Tukey; paxilline versus paxilline + RS39604, p=1; **F**, RM1WA, $F_{6,2}$=9 p = 0.005, paxilline versus control, p< 0.01, Tukey; paxilline + RS67333 versus control, p= 0.01, Tukey; paxilline versus paxilline + RS67333, p = 1).

(**C-G**) (Top) Schematic of proposed signaling elements targeted by the defined antagonists or agonists.

Figure 4

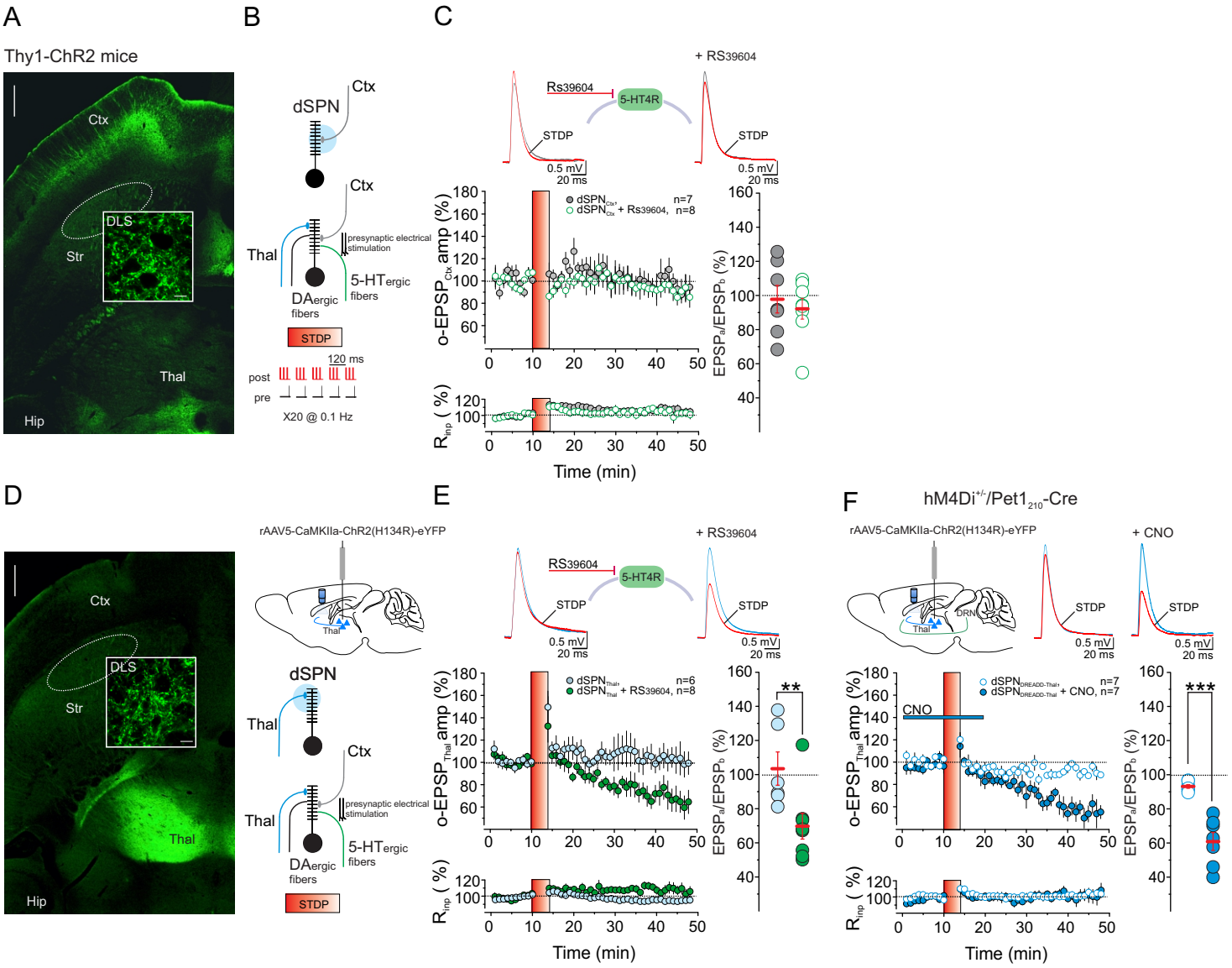
A
Thy1-ChR2 mice
Ctx
DLS
Str
Thal
Hip
B
dSPN
Ctx
Thal
presynaptic electrical stimulation
5-HTergic fibers
DAergic fibers
STDP
120 ms
post
pre
X20 @ 0.1 Hz
C
+ RS39604
Rs39604
5-HT4R
STDP
0.5 mV
20 ms
dSPNCtx, n=7
dSPNCtx + Rs39604, n=8
o-EPSPCtx amp (%)
EPSPa/EPSPb (%)
Rinp (%)
Time (min)
D
rAAV5-CaMKIIa-ChR2(H134R)-eYFP
E
RS39604
dSPNThal, n=6
dSPNThal + RS39604, n=8
o-EPSPThal amp (%)
**
F
hM4Di+/-/Pet1210-Cre
+ CNO
DRN
CNO
dSPNDREADD-Thal, n=7
dSPNDREADD-Thal + CNO, n=7
***

Figure 4. Decreased 5-HT signaling gates t-LTD at thalamo-dSPN synapses

(**A**) Confocal images of horizontal sections of Thy1-ChR2 transgenic mice; scale bar, 500 μm; Ctx, cortex; Str, striatum; Hip, hippocampus; Thal, thalamus. Inset shows ChR2-eGFP expressing axon terminals in the DLS; scale bar, 10 μm.

(**B**) Schematic of recording configuration in dSPNs. (Top) Corticostriatal stimulation evoked by 470 nm LED pulses through the microscope objective was performed before and after the STDP protocol. (Bottom) During the post-pre STDP paradigm light stimulation of cortical terminals was replaced by local electrical stimulation. (**C**) The post-pre STDP protocol failed to induce plasticity of o-EPSP$_{Ctx}$ either under control conditions (dSPN$_{Ctx}$, RM1WA $F_{6,44}$=1.1, p=0.4) or upon RS39604 application (dSPN$_{Ctx}$ + RS39604, RM1WA $F_{7,44}$=0.8, p=0.5).

(**D**) (Left and Top Right) rAAV5-CaMKIIa-ChR2(H134R)-eYFP expression targeting intralaminar thalamus (Thal); scale bar, 500 μm; Ctx, cortex; Str, striatum; Hip, hippocampus. (Inset) ChR2-eYFP^{+} axons in the DLS; scale bar, 10 μm. (Right) Schematic of recording configuration of o-EPSP$_{Thal}$ evoked by 470 nm LED pulses (Center Right), and during the delivery of the STDP paradigm (Bottom Right).

(**E**) t-LTD is induced at thalamo-dSPN synapses upon 5-HT4R inhibition (dSPN$_{Thal}$, RM1WA $F_{5,44}$=1.5, p=0.3; dSPN$_{Thal}$ + RS39604, RM1WA $F_{7,44}$=10, p=0.0002, p<0.05 Tukey; dSPN$_{Thal}$ + RS39604 versus dSPN$_{Thal}$, ** p< 0.05, Mann Whitney test).

(**F**) In hM4Di$^{+/-}$/Pet1$_{210}$-Cre mice injected with the rAAV5-CaMKIIa-ChR2(H134R)-eYFP virus, bath application of CNO (5 μM) gated t-LTD of o-EPSP$_{thal}$ in response to STDP (dSPN$_{DREADD_Thal}$, RM1WA $F_{6,44}$=1.8, p=0.1; dSPN$_{DREADD_Thal}$ + CNO, RM1WA $F_{6,44}$=10, p=0.0002, p<0.05 Tukey; dSPN$_{DREADD_Thal}$ + CNO versus dSPN$_{DREADD_Thal}$, *** p< 0.001, Mann Whitney test).

(**C**-**F**) Data are shown as time courses (mean ± s.e.m.) of normalized EPSP amplitudes and normalized Rinp. (Insets) Averaged recordings (ten traces) before (black line) and after (red

line) the delivery of the STDP protocol (red vertical bar). Scatter plot summarizes the ratios of synaptic responses after (a) and before (b) the STDP.

Figure S1

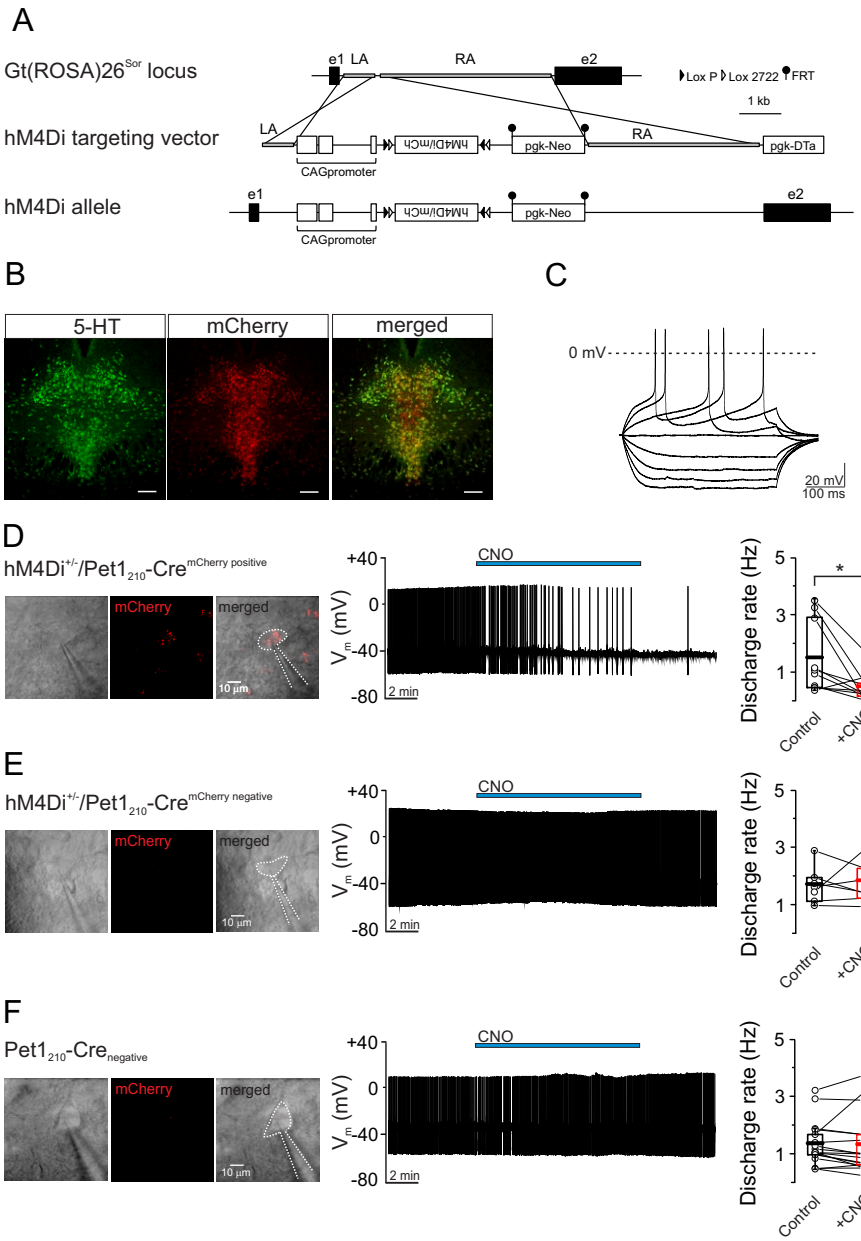
A
Gt(ROSA)26Sor locus
hM4Di targeting vector
hM4Di allele
e1
LA
RA
e2
Lox P
Lox 2722
FRT
1 kb
hM4Di/mCh
pgk-Neo
pgk-DTa
CAGpromoter
B
5-HT
mCherry
merged
C
0 mV
20 mV
100 ms
D
hM4Di+/-/Pet1210-CremCherry positive
CNO
+40
0
-40
-80
Vm (mV)
2 min
Discharge rate (Hz)
Control
+CNO
*
E
hM4Di+/-/Pet1210-CremCherry negative
F
Pet1210-Cre negative
10 µm

Figure S1, related to Figure 1. hM4Di conditional knock-in mouse line.

(**A**) Schematic of construct used to generate the hM4Di conditional knock-in mouse line. From the top to the bottom: the genomic structure of the ROSA26 locus with the homology regions highlighted that were used to prepare the hM4Di targeting vector, and the resulting hM4Di recombined conditional knock-in allele. LA: left homology arm; RA right homology arm; e1: exon 1; e2: exon 2; pgk-NEO: neomycin expression cassette containing the phosphoglicerate-kinase promoter and neomycin coding sequence; pgk-DTa: difteric toxin A expression cassette containing the phosphoglicerate-kinase promoter and difteric toxin A coding sequence; hM4Di/mCh: in-frame-fusion protein resulting from the hM4Di DREADD receptor and the mCherry reporter coding sequences.

(**B**) Double immunofluorescence analysis. Confocal images showing expression of 5-HT (green), mCherry (red) and merge in dorsal raphe nuclei (DRN) of $hM4Di^{+/-}/Pet1_{210}$-Cre mice. Scale bar, 100 μm. (**C**) DRN 5-HT neurons were identified on the basis of their current-clamp electrophysiological profile, including the lack of time-dependent depolarization (sag) in response to hyperpolarizing current pulses (400 ms long).

(**D,E**) In acute DRN brain slices from $hM4Di^{+/-}/Pet1_{210}$-Cre mice, activation of the inhibitory DREADD receptor hM4Di decreased the firing rate of $mCherry^{positive}$ 5-HT neurons (**D**) but not of $mCherry^{negative}$ 5-HT neurons (**E**). (**F**) CNO had not effect in 5-HT neurons of $Pet1_{210}$-$Cre^{negative}$ littermate animals. (**D**-**F**) (Right) Box plot summary of the changes in discharge rate in response to bath application of CNO (5 μM) in $mCherry^{positive}$ neurons (**D**; control, 1.48 ± 0.40 Hz; CNO, 0.49 ± 0.16; n = 10, *p< 0.05) and $mCherry^{negative}$ neurons (**E**; control, 1.72 ± 0.24 Hz; CNO, 1.77 ± 0.26; n = 7, p = 0.9) of $hM4Di^{+/-}/Pet1_{210}$-Cre mice and $Pet1_{210}$-$Cre^{negative}$ littermate animals (**F**; control, 1.34 ± 0.19 Hz; CNO, 1.30 ± 0.26; n = 17, p = 0.8). Values are the minimum, mean (bar inside the box), and the maximum.

Figure S2

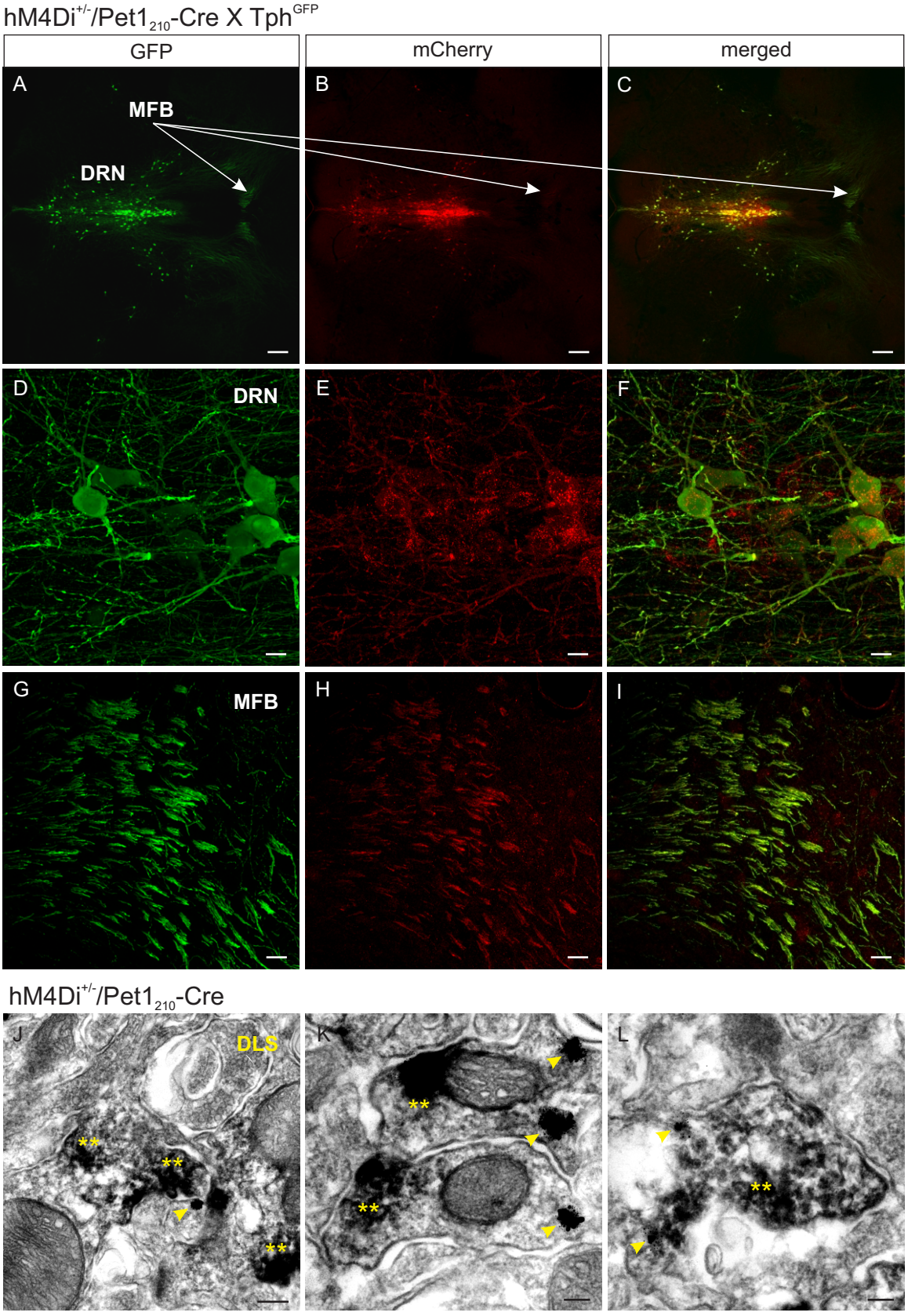
hM4Di+/-/Pet1210-Cre X TphGFP
GFP
mCherry
merged
A
B
C
MFB
DRN
D
DRN
E
F
G
MFB
H
I
hM4Di+/-/Pet1210-Cre
J
DLS
K
L

Figure S2, related to Figure 1. Expression of the hM4Di-mCherry receptor in the DRN neurons and 5-HT fibers.

(**A-C**) Confocal microscopy images of horizontal brain section of mice generated by crossing the hM4Di$^{+/-}$/Pet1$_{210}$-Cre mouse line with Tph2$^{GFP+/-}$ mice (Migliarini et al., 2013). The immunostaining for GFP and mCherry reveals the expression of the fluorescent reporters in the adult serotonergic system. (**D-F**) Confocal high magnification images confirming the presence of hM4Di-mCherry fusion protein mCherry and GFP in serotonergic neurons of the raphe nucleus and (**G-I**) in the serotonergic fibers of the medial forebrain bundle. (**J-L**) Axon fibers containing 5-HT-labelling (scattered material, yellow asterisks) and mCherry-labelling (gold particles, yellow arrowhead) in the DLS of hM4Di$^{+/-}$/Pet1$_{210}$-Cre mice. Scale bar: **A-C**, scale bar 150 μm; **D-F**, scale bar 10 μm; **G-I**, scale bar 10 μm; **J**, 200 nm; **K**,**L**, 100 nm. MFB, Medial Forebrain Bundle; DRN, Dorsal Raphe Nucleus; DLS, DorsoLateral Striatum.

Figure S3

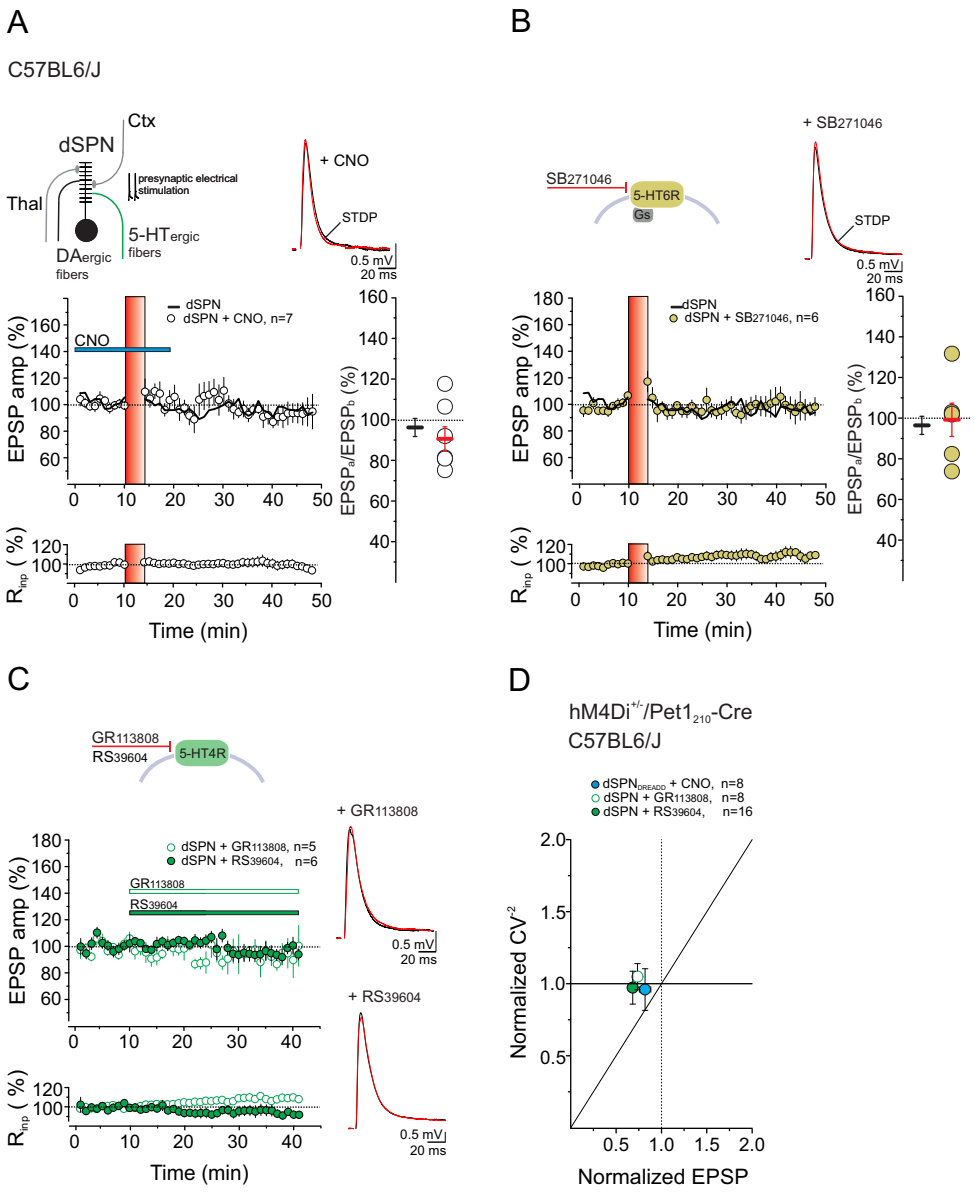
A
C57BL6/J
Ctx
dSPN
Thal
presynaptic electrical stimulation
DAergic fibers
5-HTergic fibers
+ CNO
STDP
0.5 mV
20 ms
dSPN
dSPN + CNO, n=7
CNO
EPSP amp (%)
EPSPa/EPSPb (%)
Rinp (%)
Time (min)
B
+ SB271046
SB271046
5-HT6R
Gs
STDP
dSPN
dSPN + SB271046, n=6
EPSP amp (%)
EPSPa/EPSPb (%)
Rinp (%)
Time (min)
C
GR113808
RS39604
5-HT4R
+ GR113808
dSPN + GR113808, n=5
dSPN + RS39604, n=6
GR113808
RS39604
+ RS39604
EPSP amp (%)
Rinp (%)
Time (min)
D
hM4Di+/-/Pet1210-Cre
C57BL6/J
dSPNDREADD + CNO, n=8
dSPN + GR113808, n=8
dSPN + RS39604, n=16
Normalized CV-2
Normalized EPSP

Figure S3, related to Figure 1 and Figure 2. t-LTD at glutamatergic dSPN synapses.

(**A**) In naïve mice, application of Clozapine-N-oxide (CNO, 5 μM, blue bar) during STDP did not affect glutamatergic dSPN synapses (dSPN + CNO, RM1WA $F_{6,44}$=1.5, p=0.2; dSPN + CNO versus dSPN, p=0.5, Mann Whitney test).

(**B**) The post-pre pairing protocol did not trigger plasticity in the presence of the 5-HT6R antagonist SB271046 (5 μM; RM1WA $F_{5,44}$=1, p=0.4; dSPN + SB271046 versus dSPN, p=0.9, Mann Whitney test).

(**A**,**B**) (Left) Plots show the time course of normalized EPSP amplitudes and normalized Rinp (mean ± s.e.m.). Solid black line (average) is the time course from **Figure 1B,** and reported here for comparison. (Insets, left) Recording configuration (**A**) and proposed 5-HT receptor subtype targeted by SB271046 (**B**). (Insets, right) Averaged recordings (ten traces) before (black line) and after (red line) the delivery of the STDP protocol (red vertical bar). (Right) Plots summarize the ratios of synaptic responses after (a) and before (b) the STDP.

(**C**) In the absence of coordinated postsynaptic and presynaptic activity, antagonism of 5-HT4R by GR113808 (5 μM) or RS39604 (5 μM) did not gate LTD (GR113808, RM1WA $F_{4,40}$=0.7, p=0.6; RS39604, RM1WA $F_{5,40}$=1, p=0.4). (Top), Schematic of proposed 5-HT receptor subtype targeted by the defined antagonists; (Insets, right) Averaged recordings (ten traces) before (black line) and 25 min after (red line) the application of GR113808 (white bar) or RS39604 (green bar). Data are presented as normalized EPSP amplitudes and normalized Rinp (mean ± s.e.m.).

(**D**) Variance analysis of dSPNs EPSPs suggests that t-LTD gated by decreased excitatory 5-HT signaling is expressed postsynaptically. Normalized CV^{-2} is plotted as a function of normalized EPSPs. The variation in EPSP amplitude was unchanged after t-LTD induced by the post-paring paradigm delivered in the presence of CNO (5 μM; $hM4Di^{+/-}$/Pet_{210}-Cre mice) or of the 5-HT4R antagonists GR113808 or RS39604 (5 μM; naïve mice).

Figure S4

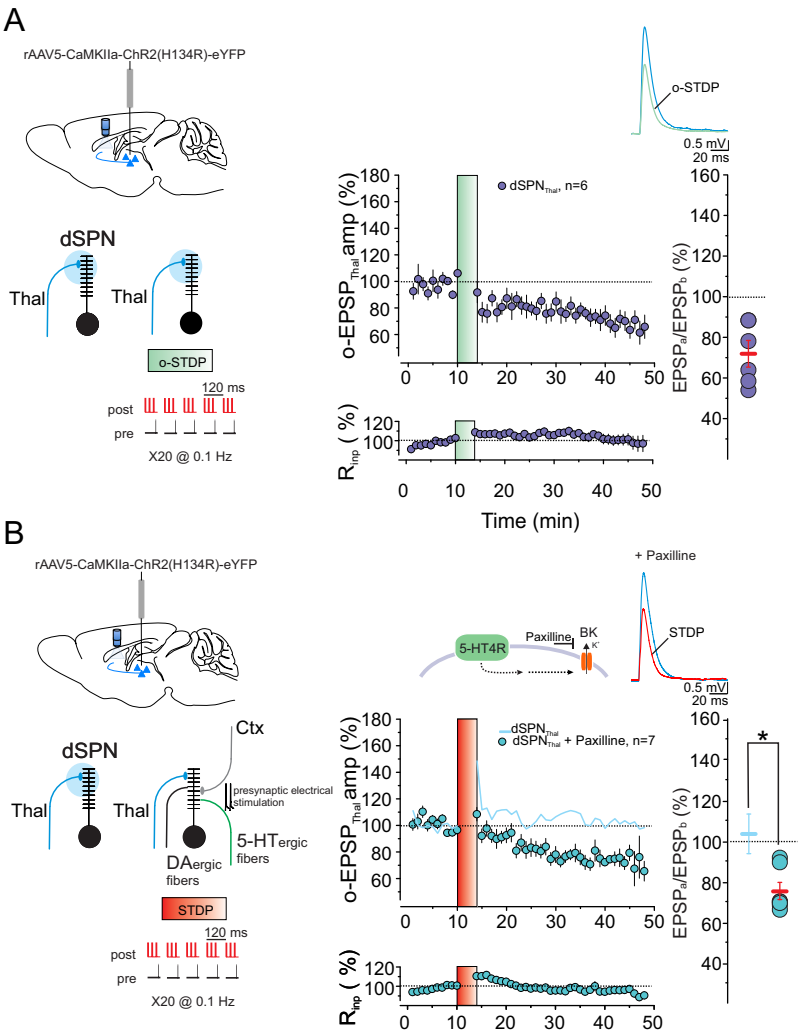
A
rAAV5-CaMKIIa-ChR2(H134R)-eYFP
dSPN
Thal
Thal
o-STDP
120 ms
post
pre
X20 @ 0.1 Hz
o-STDP
0.5 mV
20 ms
dSPN$_{Thal}$, n=6
o-EPSP$_{Thal}$amp (%)
EPSP$_a$/EPSP$_b$ (%)
R$_{inp}$ (%)
Time (min)
B
rAAV5-CaMKIIa-ChR2(H134R)-eYFP
dSPN
Thal
Thal
Ctx
presynaptic electrical stimulation
DAergic fibers
5-HTergic fibers
STDP
120 ms
post
pre
X20 @ 0.1 Hz
+ Paxilline
5-HT4R
Paxilline
BK
K+
STDP
0.5 mV
20 ms
dSPN$_{Thal}$
dSPN$_{Thal}$ + Paxilline, n=7
o-EPSP$_{Thal}$amp (%)
EPSP$_a$/EPSP$_b$ (%)
R$_{inp}$ (%)
*

Figure S4, related to Figure 4. t-LTD at thalamic inputs to dSPNs.

(**A**) (Left) Schematic of recording configuration of o-EPSP$_{Thal}$ evoked by 470 nm LED pulses, and during the delivery of the optogenetic STDP paradigm. (Right) The o-STDP protocol induced t-LTD at thalamostriatal synapses (RM1WA $F_{5,44}$=4, p< 0.0001, p< 0.05 Tukey).

(**B**) (Left) Schematic of recording configuration of o-EPSP$_{Thal}$, and during the delivery of the conventional STDP paradigm. (Right) Application of the BK channel blocker paxilline (10 μM) during the STDP paradigm is sufficient to gate t-LTD at thalamo-dSPN synapses (RM1WA $F_{6,44}$=9, p= 0.0002, p< 0.05 Tukey; dSPN$_{Thal}$ + Paxilline versus dSPN$_{Thal}$, * p< 0.05, Mann Whitney test). Solid light blue line (average) is the time course from **Figure 4E,** reported here for comparison.

(**A**-**B**) Data are shown as time courses (mean ± s.e.m.) of normalized EPSP amplitudes and normalized Rinp. (Right) Scatter plot summarizes the ratios of synaptic responses after (a) and before (b) the o-STDP (**A**) or conventional STDP (**B**). (Insets) Averaged recordings (ten traces) before and after the delivery of the o-STDP paradigm (**A**, green vertical bar) or the conventional STDP protocol (**B**, red vertical bar); Schematic in (**B**) represents the proposed signaling pathway and ion channel targeted by the defined blocker (paxilline).

References

Migliarini, S., Pacini, G., Pelosi, B., Lunardi, G., and Pasqualetti, M. (2013). Lack of brain serotonin affects postnatal development and serotonergic neuronal circuitry formation. Mol Psychiatry *18*, 1106-1118.

Supplemental experimental procedures

Drugs

Gabazine (SR95531 hydrobromide), SB271046, GR113808, RS39604, AM251, Paxilline, RS67333, AIP were purchased from Tocris Bioscience (Bristol, United Kingdom). Sodium-L-ascorbate, sodium pyruvate, $MgSO_4$, Triton X-100, NaN_3, NaCl, KCl, NaH_2PO_4, $MgCl_2$, $CaCl_2$, $NaHCO_3$, D-glucose, choline chloride, $KMeSO_4$, HEPES, Na_2-ATP, Na_3-GTP, sodium citrate, CNO (Clozapine-N-Oxide), DMSO (dimethylsulfoxide), BSA (bovine serum albumin), paraformaldehyde, glutaraldehyde, saponin were supplied by Sigma Aldrich Italia (Milano, Italy). D15 and S15 were purchased from ThermoFisher Scientific (Waltham, Massachussets) and Neurobiotin from DBA Italia (Segrate, Italy).

Animals

Male C57Bl6/J mice (postnatal day 35-80 for electrophysiology) were used in this study. Some experiments were conducted on double transgenic $hM4Di^{+/-}$/$Pet1_{210}$-Cre mice expressing the inhibitory receptor hM4Di selectively in the serotonergic neurons and on Thy1-ChR2 transgenic mice.

Generation of the hM4Di conditional knock-in mouse line

We generated the $hM4Di^{DIO}$ conditional knock-in mouse line taking advantage of a gene targeting strategy allowing the insertion of the construct via homologous recombination within the *ROSA26* genomic locus. The in-frame-fusion protein resulting from the hM4Di DREADD receptor and the mCherry reporter coding sequences was flanked by two couples of Lox sites (LoxP/Lox2722) and the resulting cassette was isoltaed from the pAAV-hSyn-DIO-*hM4Di/mCherry* vector and cloned in the 3'-5' orientation within the pCX-CAG-*eGFP* plasmid downstream to the CAG promoter by replacing the *eGFP* sequence. Subsequently,

the CAG-*hM4Di/mCherry* fragment was isolated from pCX-CAG-*hM4Di/mCherry* via SpeI/XbaI double digestion and cloned in the XbaI site of the pROSA26-1^{Sor} plasmid that was previously modified by the addition of a *PvuI* recognition site downstream to the *pgk-DTa* cassette in place of the unique XhoI site. Finally, the SpeI/NheI fragment containing the *pgk-Neo/Kana* cassette was obtained from the pPSVKeoFRT plasmid and cloned into the unique XbaI site of the pROSA26-1^{Sor}-CAG-*hM4Di/mCherry* vector.

PvuI-linearized targeting vector was electroporated in E14Tg2a.4 ES cells and G418 selection was maintained for 7 days as described (Migliarini et al., 2013). Among 192 G418-resistant ES cell colonies screened, 32 resulted positive recombinant clones as assessed by Southern Blot analysis. Following karyotype analysis, recombinant ES cells were microinjected into C57BL/6 host blastocysts that were later reimplanted into pseudopregnant CD1 females. Germline transmission was achieved for the 60% of the 29 chimeras obtained. hM4DiDIO mice born at normal Mendelian ratios and lived a normal life-span showing no obvious defects.

Animals were genotyped using DNA primers as follows: wild-type *ROSA26* allele forward 5'-GAGGGGAGTGTTGCAATACC-3' and reverse 5'-AGTCTAACTCGCGACACTGTA-3'. hM4Di^{DIO} knock-in allele we genotyped using the same forward primer as above in combination with the reverse 5'-GTCCCTATTGGCGTTACTATG-3'.

Surgeries

Five-to six-week-old mice were anesthetized (isofluorane 2%) and placed in a stereotaxic frame. To measure light-evoked EPSPs at thalamostriatal connections on dSPNs, C57Bl6/J and hM4Di$^{+/-}$/Pet1$_{210}$-Cre mice were injected with rAAV5-CaMKIIa-ChR2(H134R)-eYFP virus (UNC Vector Core, Chapel Hill, North Carolina). The parafascicular (Pf)/central medial (CM) regions of the intralaminar thalamus that project to the DS were targeted (-2.3 AP;

±0.75 LM; -3.5 DV). A volume of 0.5 µl/site of virus was injected at a rate of 0.1 µl/min. Mice were used for electrophysiological recordings 4-6 weeks after the injection.

Electrophysiology

Slice preparation

Mice were anesthetized with isofluorane and decapitated, and their brains were transferred to ice-cold dissecting artificial cerebrospinal fluid (aCSF) containing 110 mM choline chloride, 2.5 mM KCl, 1.25 mM NaH_2PO_4, 7 mM $MgSO_4$, 0.5 mM $CaCl_2$, 25 mM $NaHCO_3$, 25 mM D-glucose, 11.6 mM sodium-L-ascorbate, 3.1 mM sodium pyruvate, saturated with 95% O_2 and 5% CO_2. Coronal sections (250 µm thick) or horizontal slices (270 µm thick) were cut using a Vibratome 1000S slicer (Leica, Wetzlar, Germany), then transferred to aCSF containing 115 mM NaCl, 3.5 mM KCl, 1.2 mM NaH_2PO_4, 1.3 mM $MgCl_2$, 2 mM $CaCl_2$, 25 mM $NaHCO_3$, and 25 mM D-glucose and aerated with 95% O_2 and 5% CO_2. Following 20 min of incubation at 32 °C, slices were kept at 22–24 °C. During experiments, slices were continuously superfused with aCSF at a rate of 2 ml/min at 28 °C.

Electrophysiological recordings

Whole-cell patch-clamp recordings were made on striatal projection neurons (SPNs) of the dorsolateral striatum (DLS) in horizontal slices or in neurons of the dorsal raphe nucleus (DRN) in coronal slices. Intracellular solution contained (in mM): 135 $KMeSO_4$, 10 KCl, 10 HEPES, 1 $MgCl_2$, 2 Na_2-ATP, 0.4 Na_3-GTP (pH 7.2-7.3, 280-290 mOsm/kg). In the DLS, excitatory postsynaptic potentials (EPSPs) were evoked in the presence of the $GABA_A$ receptor antagonist gabazine (10 µM) by intrastriatal electrical stimulation using a concentric bipolar electrode (20-80 µA; 40-60 µs; FHC, Bowdoin, Maine) or by optogenetic stimulation of cortical or thalamic afferents using short blue light pulses (range 0.1-1 ms at 470 nm) of LED light delivered through the microscope objective (CoolLED, pE-100, Andover,

Hampshire, United Kingdom). STDP-LTD was induced using a protocol consisting of 20 bouts of EPSPs paired with bAPs, delivered 10 s apart. Each bout consisted of five bursts (120 ms apart) each composed of three bAPs at 50 Hz followed by one EPSP (negative timing). The onset of the EPSPs followed the peak of the last postsynaptic action potential in the burst by 10 ms (Δt =10 ms). During plasticity induction, postsynaptic neurons were depolarized from −80 mV to −70 mV.

Imaging

Ca^{2+} transients were imaged with 100 μM Fluo-4 (Life Technologies, Carlsbad, California) dissolved in the intracellular recording solution. Alexa 568 (10 μM, Invitrogen, Carlsbad, California) was used for visualization of cell bodies and dendrites. SPNs were filled with Alexa 568 and Fluo-4 via the patch electrode for 20 min before imaging to allow dye equilibration in the proximal dendrites. Whole cell maximum-projection images of the soma and dendrites were acquired with 0.4 μm^2 pixels with 15 μs pixel dwell time; ~120 images were taken with 0.4 μm focal steps. Drugs were bath applied for 10 min.

Two-photon Ca^{2+} imaging was performed with a Leica SP5 AOBS upright DM6000 CFS microscope coupled with a 2P laser Chameleon Ultra Coherent and equipped with a Leica 25x NA 0.95 water-immersion objective. For all experiments, the laser wavelength was 800 nm. The fluorescence emission was collected with an external non-descanned photomultiplier detector equipped with a 525/50 emission filter.

Green fluorescence line-scan signals were acquired at 6 ms and 256 pixels per line, with 0.1 μm pixels and 20 μs pixel dwell time. The laser-scanned images were acquired with 800 nm light pulsed at 90 MHz (pulse duration: ~250 fs). The line scan was used to record the fluorescence elicited by one bout of the STDP protocol.

Images were collected with LAS AF Leica software and analyzed using ImageJ software (version 1.45, http://rsb.info.nih.gov/ij/, NIH, Maryland) and Origin 9.1 (OriginLab Corporation, Northampton, Massachussets).

For each recording, background fluorescence was determined from a cell-free area of comparable size to that of the line-scan image. After subtracting the averaged background signal, fluorescence values were recorded for 200 ms before the triggering of the STDP protocol and averaged to give the basal fluorescence (F_{basal}). The amplitude of the fluorescence transients at the recording sites was expressed as the fractional change in basal fluorescence, $(F-F_{basal})/F_{basal,}$ ($\Delta F/F$), which is approximately proportional to the changes in intracellular Ca^{2+}. Over the course of the experiment, F_{basal} remained within the standard error of F_{basal} measured under control conditions. For data analysis, transients were digitally filtered off-line (adjacent-averaging routine, smoothing factor n = 5; Origin 9.1).

Immunofluorescence

Identification of dSPNs

To identify striatonigral neurons, SPNs were filled with Neurobiotin (0.5 mg/ml, DBA Italia, Segrate, Italy) during recordings and subsequently processed for immunostaining against A2A receptor (marker of neurons of the indirect pathway, iSPNs) and substance P (marker of dSPNs)(Nazzaro et al., 2012; Trusel et al., 2015). After the recording, slices were fixed with 4% paraformaldehyde in 0.1 M phosphate buffer (0.1 M PB; pH 7.4) overnight at 4 °C and then incubated in primary antibodies. Rabbit polyclonal antibody to A2A (1:250, Enzo Life Sciences, Farmingdale, New York) or rat monoclonal antibody to substance P (1:200, Millipore, Billerica, Massachussets) were diluted in 0.1 M PB containing 0.3% Triton X-100. Sections were subsequently incubated with Alexa 647- or Alexa 488-conjugated secondary antibodies (1:200) and Alexa 568-conjugated streptavidin (1:1000) (Invitrogen, Carlsbad,

California), mounted on glass slides, and coverslipped with ProLong Gold antifade reagent (Invitrogen, Carlsbad, California). Images were acquired with an inverted confocal microscope Leica TCS SP5 AOBS TANDEM.

Immunofluorescence for 5-HT and mCherry expression

Mice were perfused with 4% paraformaldehyde (w/v) in phosphate buffer (0.1 M PB; pH 7.4) and vibratome sections (50 μm) were processed for immunofluorescence (Migliarini et al., 2013). After blocking and permeabilization, slices were incubated in primary antibody [rabbit anti-RFP antibody (1:500, Abcam, Cambridge, United Kingdom); chicken polyclonal anti-eGFP antibody (1:1000, Abcam, Cambridge, United Kingdom); rat polyclonal anti-5HT (1:200, ThermoFisher Scientific, Waltham, Massachussets)] overnight at 4 °C. Slices were then incubated in secondary antibody [Oregon Green 488 goat anti- chicken IgG (1:500, Molecular Probes, Eugene, Oregon); VectaFluor™ Excel Amplified DyLight® 594 Anti-Rabbit IgG Kit; Alexa Fluor 488 donkey anti- rat IgG (1:500, Molecular Probes, Eugene, Oregon)] for 1 hr at room temperature and mounted onto slides for imaging. Images were acquired by MacroFluo microscope (Leica, Weltzar, Germany) with DS-SMc digital cameras (Nikon, Tokio, Japan) or A1 confocal microscope (Nikon, Tokio, Japan).

Immuno EM analysis

The pre-embedding immuno-gold analyses were performed as described (Hebert-Chatelain et al., 2014). In short, after a pre-incubation step in blocking solution [(10% BSA, 0.1% sodium azide and 0.02% saponin in Tris Buffered Saline (TBS)] coronal sections were incubated with a rat monoclonal anti-mCherry (1:50, Sigma Aldrich Italia, Milano, Italy) and a rabbit polyclonal anti-5HT (1:200, ThermoFisher Scientific, Waltham, Massachussets) primary antibodies in blocking solution with 0.004% saponin. After several washes (1% BSA in TBS), sections were incubated with a goat anti-rabbit biotinylated secondary antibody (1:150,

Vector Laboratories, Peterborough, United Kingdom) and with secondary 1.4 nm gold-labeled goat anti-rat Immunoglobulin-G (Fab' fragment, 1:100, Nanoprobes Inc., Yaphank, New York). Sections were then processed in avidin-biotin complex (1:50, Vector Laboratories, Peterborough, United Kingdom), silver intensified with the HQ Silver kit (Nanoprobes Inc., Yaphank, New York), and incubated in a solution 0.05% DAB and 0.01% hydrogen peroxide (Vector Laboratories, Peterborough, United Kingdom). After post fixation with 1% glutaraldehyde, the immunolabeled, sections were analyzed by electron microscopy, as described (Giacomini et al., 2016). Scanning transmission electron microscopy (STEM) images were collected with a Schottky field-emission gun FEI Tecnai G2 F20 (FEI, Hillsboro, Oregon) transmission electron microscope equipped with a high angular annular dark field (HAADF) detector and operating at an acceleration voltage of 200 kV.

References

Giacomini, C., Mahajani, S., Ruffilli, R., Marotta, R., and Gasparini, L. (2016). Lamin B1 protein is required for dendrite development in primary mouse cortical neurons. Mol Biol Cell *27*, 35-47.

Hebert-Chatelain, E., Reguero, L., Puente, N., Lutz, B., Chaouloff, F., Rossignol, R., Piazza, P.V., Benard, G., Grandes, P., and Marsicano, G. (2014). Cannabinoid control of brain bioenergetics: Exploring the subcellular localization of the CB1 receptor. Mol Metab *3*, 495-504.

Migliarini, S., Pacini, G., Pelosi, B., Lunardi, G., and Pasqualetti, M. (2013). Lack of brain serotonin affects postnatal development and serotonergic neuronal circuitry formation. Mol Psychiatry *18*, 1106-1118.

Nazzaro, C., Greco, B., Cerovic, M., Baxter, P., Rubino, T., Trusel, M., Parolaro, D., Tkatch, T., Benfenati, F., Pedarzani, P., *et al.* (2012). SK channel modulation rescues striatal plasticity and control over habit in cannabinoid tolerance. Nature neuroscience.

Trusel, M., Cavaccini, A., Gritti, M., Greco, B., Saintot, P.P., Nazzaro, C., Cerovic, M., Morella, I., Brambilla, R., and Tonini, R. (2015). Coordinated Regulation of Synaptic Plasticity at Striatopallidal and Striatonigral Neurons Orchestrates Motor Control. Cell Rep *13*, 1353-1365.